7700 Years of Holocene Climatic Variability in Sermilik Valley, Southeast Greenland Inferred From Lake Sediments

7700 YEARS OF HOLOCENE CLIMATIC VARIABILITY IN SERMILIK VALLEY, SOUTHEAST GREENLAND INFERRED FROM LAKE SEDIMENTS

A Thesis Presented

By

SAMUEL HALLETT DAVIN

Submitted to the Graduate School of the

University of Massachusetts in partial fulfillment

of the requirements for the degree of

MASTER OF SCIENCE

May 2013

GEOSCIENCES

7700 YEARS OF HOLOCENE CLIMATIC VARIABILITY IN SERMILIK VALLEY, SOUTHEAST GREENLAND INFERRED FROM LAKE SEDIMENTS

A Thesis Presented

By

SAMUEL HALLETT DAVIN

Approved as to style and content by:

_____
Raymond S. Bradley, Chair

_____
Nicholas Balascio, Member

_____
Julie Brigham-Grette, Member

_____
R. Mark Leckie, Department Head
Department of Geosciences

ACKNOWLEDGEMENTS

There are a great number of people to whom I owe thanks for their love, assistance, input, and camaraderie, and I lament that not all of those who deserve praise can be mentioned herein. I would first like to thank Professor Raymond Bradley for his patience and support throughout this project, for without him none of this work would have been possible. I would also like to thank Ray for sending myself and Greg de Wet to Greenland in the summer of 2012 to conduct geologic research. My time spent in Greenland was among the best experiences of my life, and for that I will be forever grateful. To Nicholas Balascio I extend great thanks for his assistance both in and out of the laboratory over the past four years, and for acting as an exemplary scientific mentor and role model. To my graduate student cohort and constant competitor, Greg de Wet, I cannot say enough. Never before have I had a chance to work alongside another with such enthusiasm, drive, and passion for paleoclimatology. Most of all I would like to thank Greg for his sense of honor and decency.

I would also like to thank my parents, Daniel and Virginia, for raising me to appreciate the natural world. To my mother I owe special thanks for reading rock and mineral guides to me each night as a child. To my grandmother I am forever indebted for introducing me to the field of geology so early in my life. Finally, I would like to acknowledge Kat Dolan for the incredible support she has provided over the past two years. Kathleen, you are a rare human being indeed.

ABSTRACT

7700 YEARS OF HOLOCENE CLIMATIC VARIABILITY IN SERMILIK VALLEY, SOUTHEAST GREENLAND INFERRED FROM LAKE SEDIMENTS

MAY 2013

SAMUEL H. DAVIN, B.S., UNIVERSITY OF MASSACHUSETTS AMHERST

M.S., UNIVERSITY OF MASSACHUSETTS AMHERST

Directed by: Professor Raymond S. Bradley

During the latter half of the 20th century until present day there has been an unprecedented rise in global annual mean temperatures accompanied by rising sea levels and a decrease in Northern Hemisphere snow cover, which if it continues will lead to widespread disruption of climate patterns, ecosystems, and present-day landscapes. It is therefore of critical importance to establish an expanded network of paleoclimate records across the globe in order to better assesses how the global climate system has changed in the past, that we may create a metric by which to address modern change. Herein is presented a 7,700 years record of Holocene climatic and environmental variability in Sermilik Valley, located on Ammassalik Island, SE Greenland. This objective of this study is to determine the timing of major Holocene climate transitions as expressed in the physical, elemental, and geochemical parameters preserved in the 484 cm sediment record of Lower Sermilik Lake. Major transitions observed in this study include the deglaciation of Sermilik Valley, the onset and termination of the Holocene Climatic Optimum, the transition into neoglacial conditions, and the Little Ice Age.

TABLE OF CONTENTS

LIST OF FIGURES

CHAPTER 1

INTRODUCTION

1.1 Context

During the latter half of the 20th century until present day there has been an unprecedented rise in global annual mean temperatures accompanied by rising sea levels and a decrease in Northern Hemisphere snow cover, which if it continues will lead to widespread disruption of climate patterns, ecosystems, and present-day landscapes. It is therefore of critical importance to establish an expanded network of paleoclimate records across the globe in order to better assesses how the global climate system has changed in the past, that we may create a metric by which to address modern change.

Lake sediments provide unique records of environmental variability, including climate signals. Marine sediments, though unparalleled in recording global climate signals, can match neither the resolution nor the unique regional aspects of climate signals recorded in lakes. Similarly, highly-resolved ice cores are invaluable for purposes such as measuring concentrations of atmospheric gases and inferring conditions on ice sheets, but fall short of capturing true past terrestrial conditions. For these reasons climate signals recorded in the subaqueous sediments of lakes add an important dimension to our understanding of natural climatic variability, and provide a means of reconstructing climates of the past as well as assessing the impacts of climate change on lake systems themselves. Of particular interest are lakes situated at high latitudes, whose susceptibility to climate change is great due to polar amplification, the resultant of positive feedbacks in the climate system (e.g. Moritz et al., 2002). Furthermore, in such high latitude regions the study of lake sediments may at times be the only viable means of establishing

terrestrial records of environmental and climate change, as some proxy methods such as tree-ring analysis and palynology become difficult to successfully use in tundra environments. This highly-resolved paleolimnological study comes at a time when there is a necessity to expand our understanding of the natural variability of Earth's climate on timescales meaningful to humans.

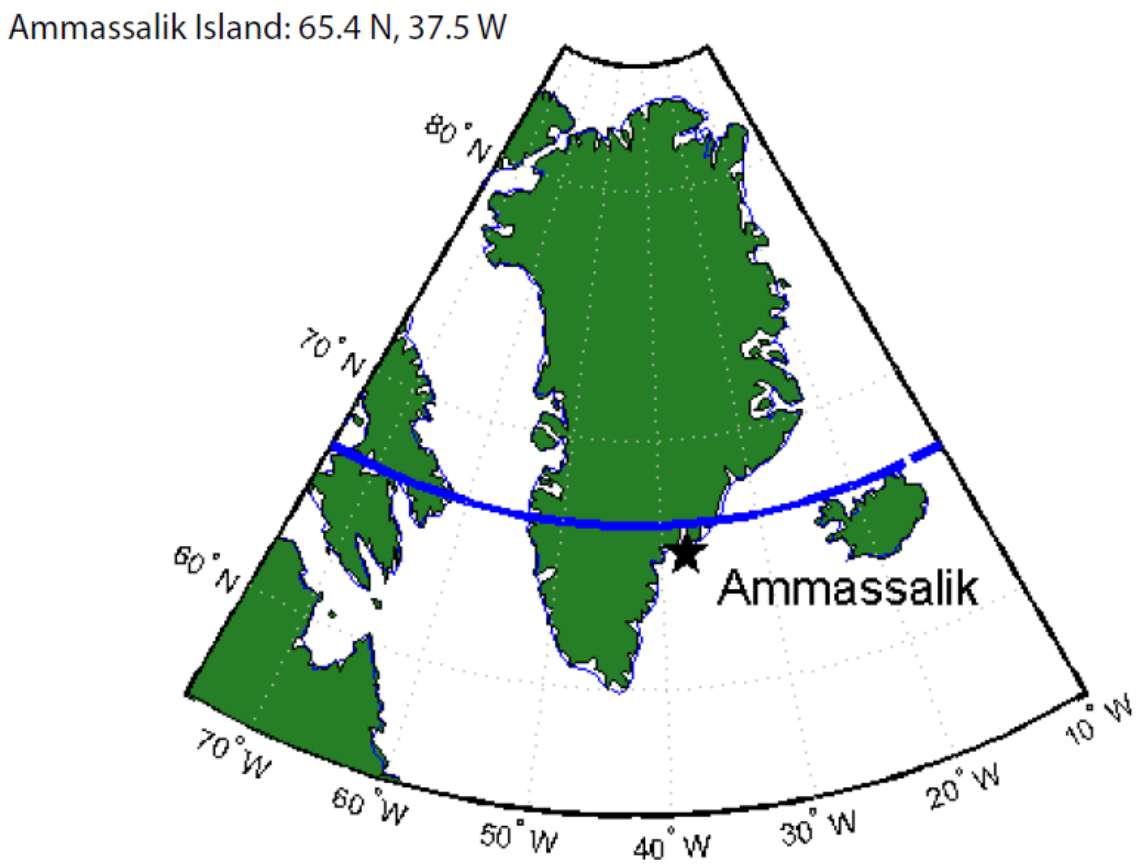

Figure 1: Ammassalik Island is located on the eastern coast of Greenland at 65.4° N, 37.5° W. The Arctic Circle is denoted as a blue line.

1.2 Study Location

Ammassalik Island in Southeast Greenland and the area of study, Lower Sermilik Lake, are situated at 65.4° N and 37.5° W (Figure 1). Ammassalik Island has an area of

~772 km^2 and is home to Tasiilaq, the largest settlement in East Greenland with a population of 1,930 as of 2010. The landscape is dominated by mountains, valleys, and freshwater. The landscape, though initially driven by tectonism and metamorphic activity, bears the hallmarks of Holocene and Pleistocene glacial erosion. Perennial ice persists in the Mittivakkat glacier, which is the largest contiguous ice field on Ammassalik Island. About two thirds of the island is dominated by ice and snow fields, while the remaining third is a mixture of bare rock, lakes, shrub and grass-covered topsoil, and glacial and fluvial deposits. Ammassalik Island provides a climatically fascinating backdrop to this study because of its close proximity to the Atlantic Ocean to the south and west, and to the Greenland Ice Sheet to the north and east.

1.2.1 Modern Ammassalik Climate

The climate of Ammassalik Island is low arctic maritime, with a mean[1895-2010] winter (December, January, February) temperature[1] of -7.1° C, and a mean[1] summer (June, July, August) temperature of 6.6° C. Annual precipitation[1] averages approximately 870 mm , with winter precipitation being somewhat greater than summer precipitation (Figure 2). These data have been obtained from a Weather Station situated on Ammassalik Island in the settlement of Tasiilaq.

The climate of southeast Greenland is strongly influenced by the polar waters of the East Greenland Current (EGC) and by the relatively warmer waters of the Irminger Current (IC). The influence of each respective current has evolved throughout the duration of the Holocene (e.g. Massa et al. 2011); though disentangling the influences of these changes from external forcings such as the decrease in insolation since the early Holocene or influxes of melt water from the Laurentide Ice Sheet proves difficult. The

Atlantic Multidecadal Oscillation (AMO), a mode of variability occurring in the North Atlantic Ocean expressed principally in sea surface temperature (SST) likely plays a large role in influencing climate conditions on Ammassalik Island, notably in terms of glacial melt (e.g. Mernild et al. 2011). As a potential control on fluvial and groundwater processes, positive AMO periods may be expressed in terms of higher-than-normal energy transport to lake catchments and therefore be reflected in larger grain sizes or higher amounts of terrestrially-derived minerals.

Another factor worthy of consideration is the influence of atmospheric oscillations such as the North Atlantic Oscillation (NAO) or Atlantic Multidecadal Oscillation (AMO) on the development of terrestrial conditions in coastal East Greenland, and what controls these effects had on the biosphere, hydrosphere, and geosphere both locally and regionally. For instance, today during negative phases of the NAO, northern Europe and Scandinavia typically receive less precipitation, while southern and central Europe receive more (Hurrell 2003). In positive phases of the NAO, the Azores High pressure center strengthens and the Icelandic low pressure center weaken further, resulting in a much greater pressure difference between the two locations. The result is higher temperatures in the Eastern US and northern Europe, colder temperatures in Greenland, more precipitation in northern Europe and Scandinavia, and less precipitation in central and southern Europe (Hurrell 2003).

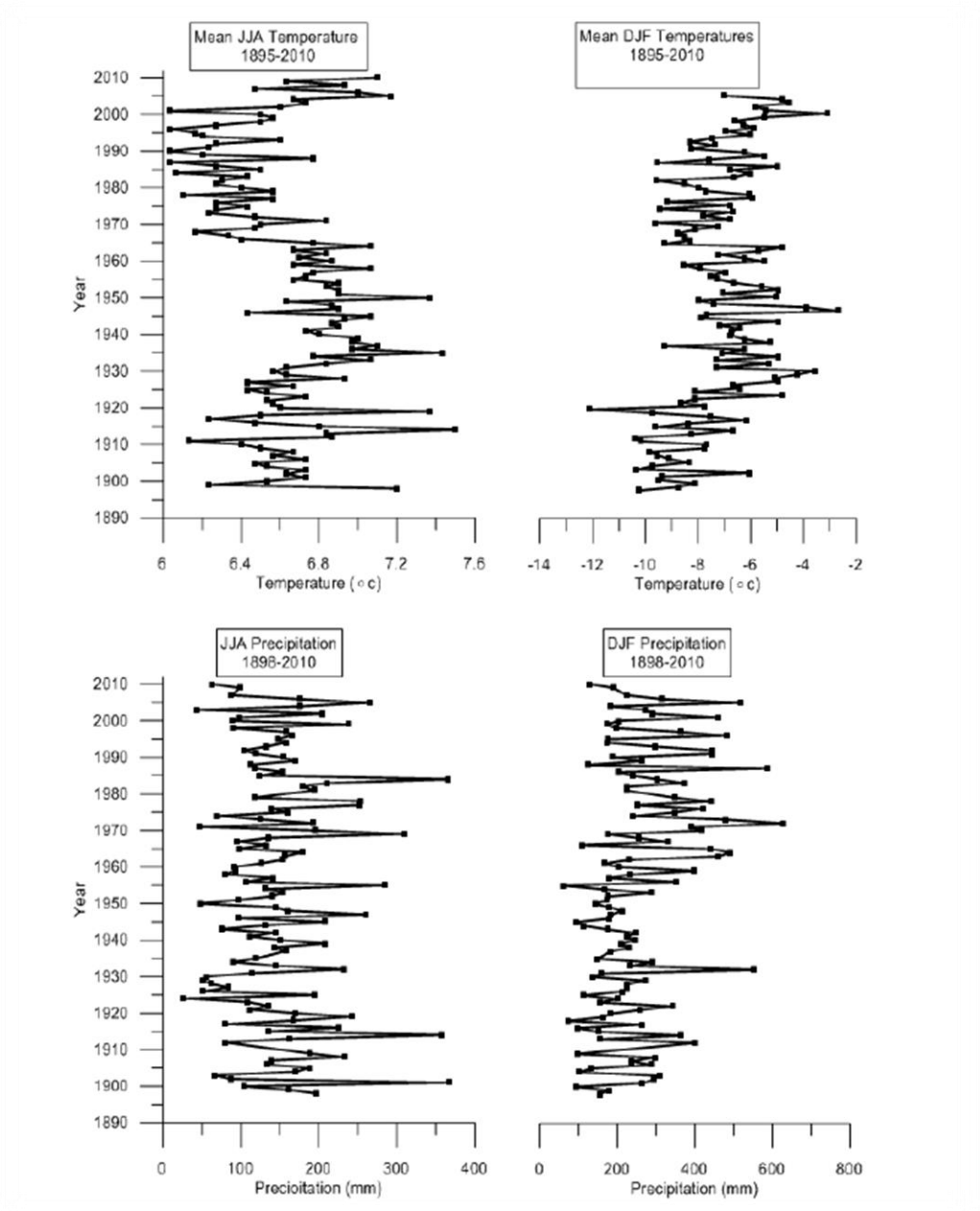

Figure 2. Mean annual summer (June, July, August) and winter (December, January, February) instrumental temperature and precipitation data for Ammassalik Island, collected since 1895 and 1898 respectively. Data were obtained from a weather station based out of Tasiilaq. The mean summer temperature is 6.6°C and the mean winter temperature is -7.1°C. The mean annual precipitation is 870 mm, much of which is received during the winter as snowfall.

1.2.2 Bedrock Geology

The area of study is located in the Nagssuqtoquidan mobile belt, primarily consisting of Archean granite gneiss. These rocks have been partially reworked by belts of intense deformation during the Proterozoic, before and after which swarms of mafic dikes intruded the area. In zones unaffected by shear belts the Archean gneisses are clearly observed to consist of a layered sequence of quartzo-feldspathic gneisses dominated by granodiorite and tonalite gneisses containing intrusions of mafic and ultramafic material interleaved with supracrustal sequences and anorthisites (Bridgewater, 1976). The predominant unit of the Lower Sermilik catchment is a major charnockite complex bordered by garnet-rich county rock extending from the west coast of Sermilik fjord through the southern part of Ammassalik (Figure 3) (Wager, 1934).

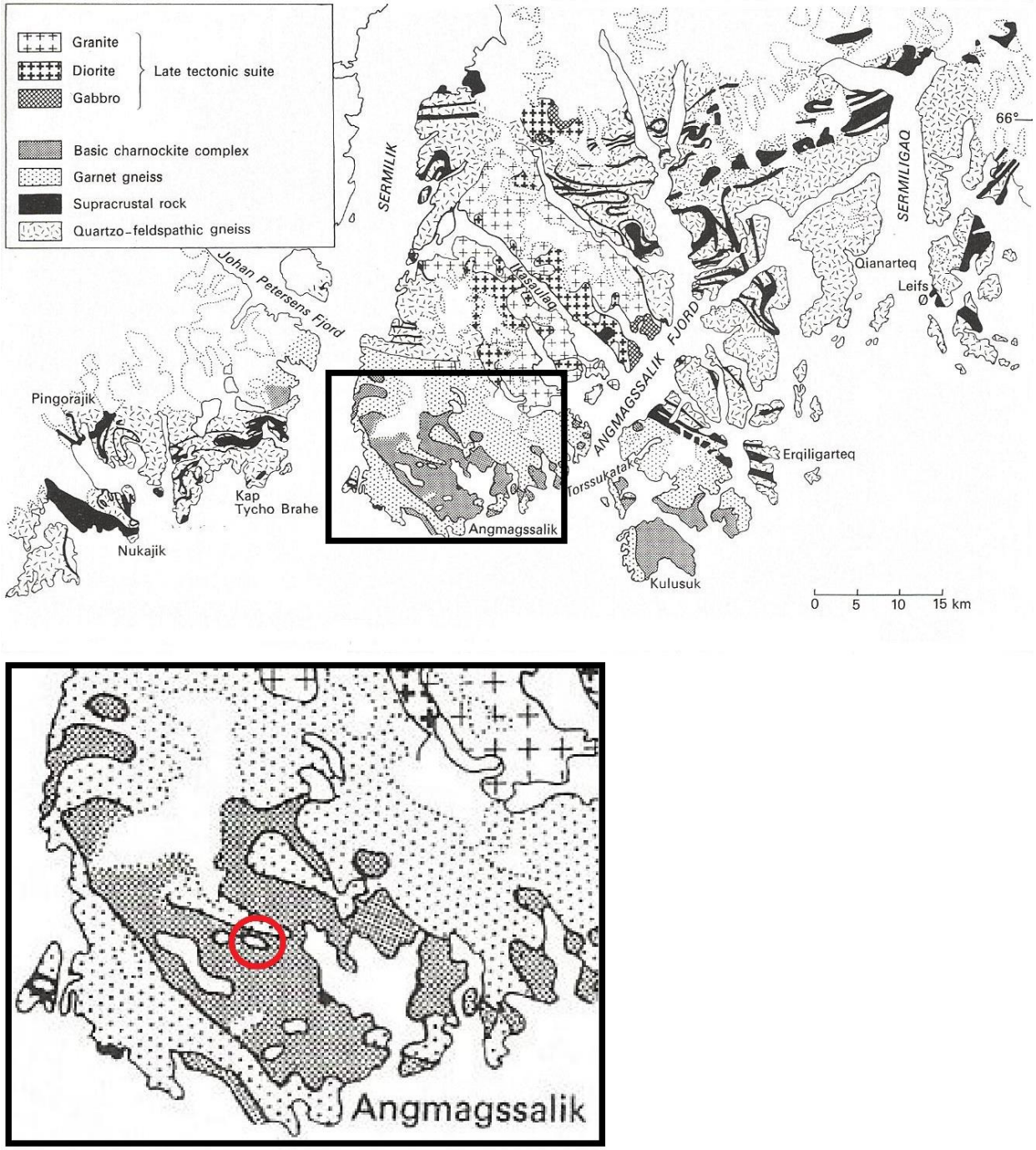

Figure 3. Geologic map of Ammassalik Island adapted from "Geology of Greenland", by Escher & Watt. Lower Sermilik is circled in red. The catchment of Lower Sermilik isunderlain by basic charnockite and garnet gneiss.

1.2.3 Lower Sermilik Lake and Catchment

Lower Sermilik (65°38’40” N, 37°43’27” W) is located in the Sermilik Valley on Ammassalik Island in the Sermersooq municipality of Southeast Greenland **(**Figure 1, Figure 5**).** Along its southern banks Lower Sermilik is bordered by the steep talus slopes of the spiny Præstefjeld ridge (641 masl), by Upper Sermilik Lake and the Mittivakkat Glacier to the west, by grassy slopes and bare-rock peaks to the north, and by a long, gentle, grassy slope terminating in Tasiilaq Fjord 1.4 km to the east (see Figure 5). The banks of Lower Sermilik sit at 70 meters above sea level (m asl), and bathymetric surveys of the lake reveal a maximum depth of 30 m (Figure 4). The color of Lower Sermilik, as of July, 2012, was observed to be a dark shade of turquoise, very clear, and cold. Biogeochemical and sedimentological assessments of Lower Sermilik find it to provide a continuous sediment record since ~7200 cal yr BP, likely when perennial glacial ice persisting from the Younger Dryas retreated beyond the lake margin. Since this record is interpreted to be continuous since the time of local deglaciation it stands to reason that a record of climate and environmental change may be recovered from these sediments for the middle Holocene onward.

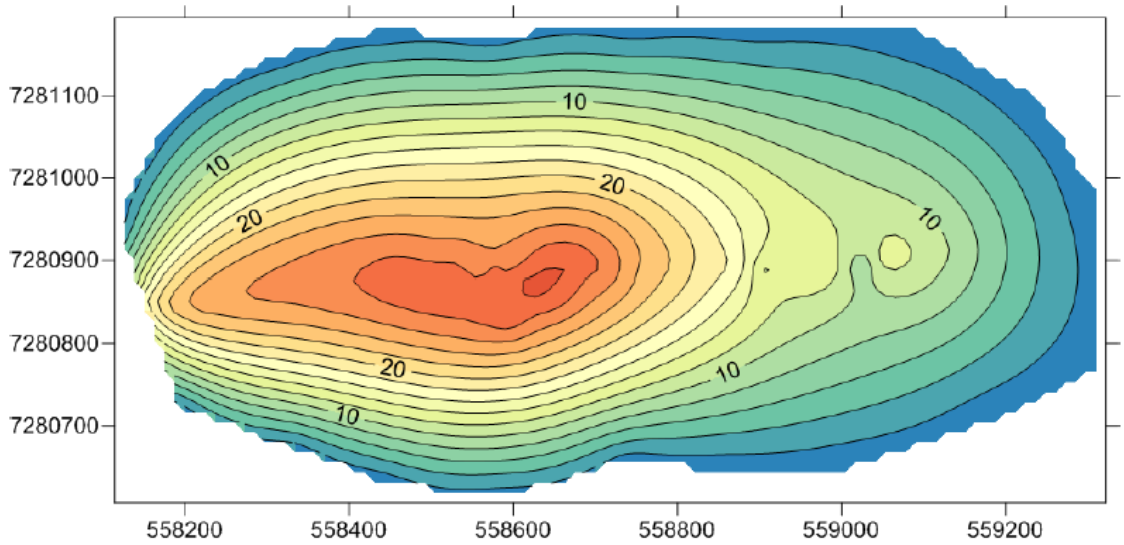

Figure 4. Bathymetric profile of Lower Sermilik oriented south. The contour interval is 2 meters. Cores were collected from the deepest portion of the lake (~30 m)

In order to understand biological and geological processes operating within and around Lower Sermilik, it is of importance to understand its sister lake, Upper Sermilik. Upper Sermilik is at 148 m asl, approximately 0.4 km from the western terminus of Lower Sermilik. With a comparably small catchment area of ~5.3 km^2, Upper Sermilik is fairly isolated within Sermilik Valley by steep slopes. It receives surficial flow from proximal snow melt and precipitation events, and also from a turbid channel fed by a cascading waterfall sourcing from the Mittivakkat Glacier, which before emptying into Upper Sermilik, opens into a massive alluvial fan. The suspended sediment load of this channel is great, and can be visibly noted by the stunning turquoise color of this lake and by the visible ~1000 m long sediment plume entering the lake from the mouth of the primary alluvial fan channel.

Both Lower Sermilik and sister lake Upper Sermilik sit in the glacially-carved Sermilik Valley (Figure 5), which acts much as a gutter collecting runoff from both proximal snow melt and precipitation events, as evidenced by plentiful dry and active erosional channels. The catchment of Lower Sermilik is estimated to be 9.5 km^2. With the exception of runoff from the surrounding slopes, Lower Sermilik is fed by two primary sources: source one is Upper Sermilik, which is connected to Lower Sermilik via a narrow passage cut through a bedrock ridge. This rapidly flowing channel measures approximately 2 meters wide by 1 meter deep, and experiences several small drops before opening into an alluvial fan comparable to the size of the fan at Upper Sermilik. The second source is a steep and rapidly-flowing melt water channel water from a smaller lake (200 m wide by 600 m long) located in a massive cirque to the North. This channel cuts through the crystalline bedrock to depths of greater than 1 meter in some locations, suggesting this lake has been present for quite a long time, perhaps even sub-glacially or during ice retreat. This source has also formed a large alluvial fan, which is adjacent to the other. This fan is larger and a steady series of meandering, braded streams cut through it before emptying into Lower Sermilik.

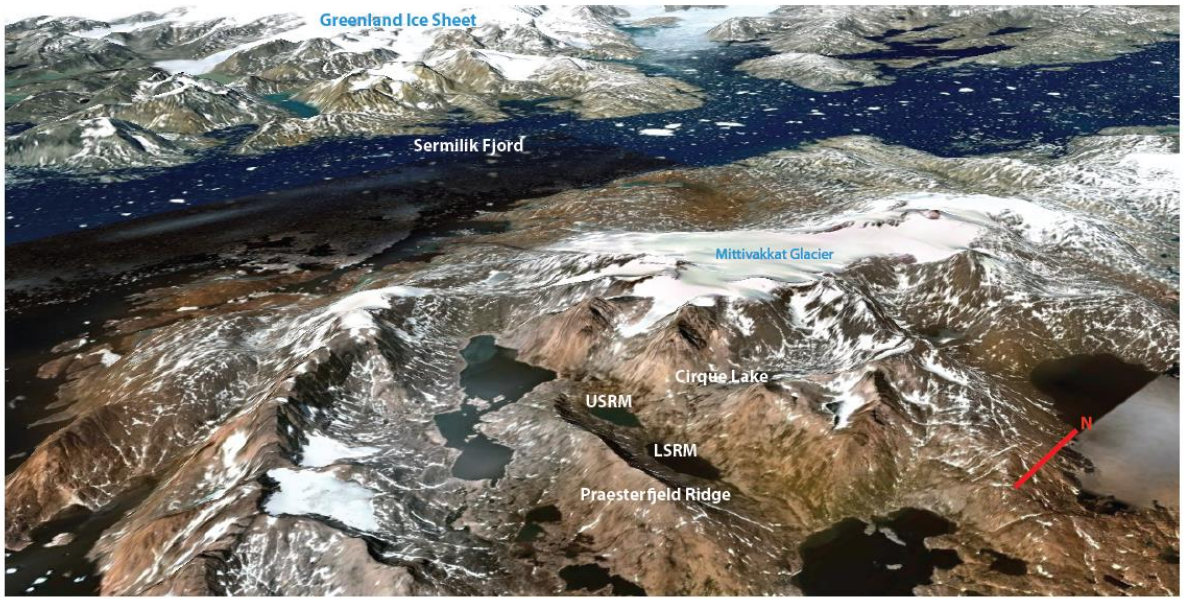

Figure 5. An aerial view of the southwestern quadrant of Ammassalik Island oriented Northwest, with major features labeled. Lower Sermilik is labeled as "LSRM" and Upper Sermilik is labeled as "USRM". The Atlantic Ocean is not pictured, but is located immediately to the South and to the East of Ammassalik Island. Tasiilaq is located several kilometers to the southwest of Lower Sermilik

1.3 Previous work

To date no scientific research involving Lower Sermilik Lake has taken place, however several studies have been carried out on Ammassalik Island. Christiansen et al., (1999) and Humlum et al., (2008) explored the geomorphology of Ammassalik Island by combining analyses of sediments with ^{14}C and optically stimulated luminescence dating to determine paleo-prevailing wind directions, eustasy, and the onset of abrupt changes including the Little Ice Age. Findings indicate strong, persistent northeasterly winds throughout much of the Holocene. In the findings of Humlum et al. (2008) the Mittivakkat Glacier, located just northwest of Lower Sermilik, appeared 3,000-4,000 years BP during the onset of neoglacial conditions. Hasholt and Mernild (2008) investigated the hydrology and sediment transport of Ammassalik Island with a particular

focus on modern water resources available to the indigenous population. Jakobsen et al., (2008) explored changes in vegetation on Ammassalik Island recorded in lake sediments and soil profiles.

Other paleolimnological studies on Greenland have been carried out, although these studies did not take place near Ammassalik. Willemse et al., (1999), Cremer et al. (2001), Wagner et al., (2000), Wagner et al., (2002), Andreson et al., (2004), Klug et al., (2008), Klug et al., (2009) all investigated the Holocene climate history of Greenland using lake sediments. Willemse, et al. (1999) presented data derived from West Greenland lake records, Cremer et al., examined diatom succession in an East Greenland lake, Wager et al., (2000) explored paleolimnologic findings from lakes in West Greenland and Wager et al., (2002) explored paleolimnologic records from lakes in Northeast Greenland, as did Klug et al., (2008) and Klug et al., (2009). Andreson et al., (2004) investigated Holocene climatic changes in southern Greenland using biogeochemical and sedimentological data. Though these findings are certainly of interest, they focus on locations far from Lower Sermilik.

CHAPTER 2

MATERIALS & METHODS

2.1 Core Collection and Field Assessment

In the spring of 2010 a research team consisting of Dr. Raymond Bradley, Dr. William D'Andrea, Dr. Nicholas Balascio, and Dr. Lucien von Gunten visited four lakes in Southeastern Greenland including Lower Sermilik. Two cores consisting of three drives each and were collected from Lower Sermilik using a tripod-mounted percussion coring rig. Two additional surface gravity cores were taken as well to ensure that the sediment-water interface was captured. The team also collected conducted bathymetry transects **(**see figure 5**)** and took measurements of water temperature, pH, and salinity incrementally through the water column (Figure 6).

In July of 2012 the author Samuel Davin and graduate student co-collaborator Greg de Wet returned to Lower Sermilik and collected surface sediments from the lake, soil samples from the catchment, and vegetation samples from the catchment. Care was taken to create detailed surficial maps and to examine all channels (flowing or otherwise) within the catchment. The three days spent investigating Lower Sermilik yielded sufficient evidence to infer the glacial history of Sermilik Valley in which Lower Sermilik resides.

2.2 Composite Core Description

The composite core from Lower Sermilik is 484.5 cm, and uses 8 cm of material from the surface core LSRM-10-D-C in addition to the three A-core sections (LSRM-10G-A1, LSRM-10G-A2, AND LARM-10G-A3), and two of the three B-core sections (LSRM-10G-B2 and LSRM-10G-B3). Core sections LSRM-10-D-C, LSRM-10G-A1 and

LSRM-10G-A2 are characterized by thick laminations of similar color interspersed with zones of slumped material, though the laminations of LSRM-10G-A2 begin to fine and darken towards the base of the section. Core sections LSRM-10G-B2 AND LSRM-10G-A3 are characterized by fine laminations with notable color variation between laminations. LSRM-10G-B3 is characterized by clay, coarse sand, and cobbles up to 5 cm across the z-axis.

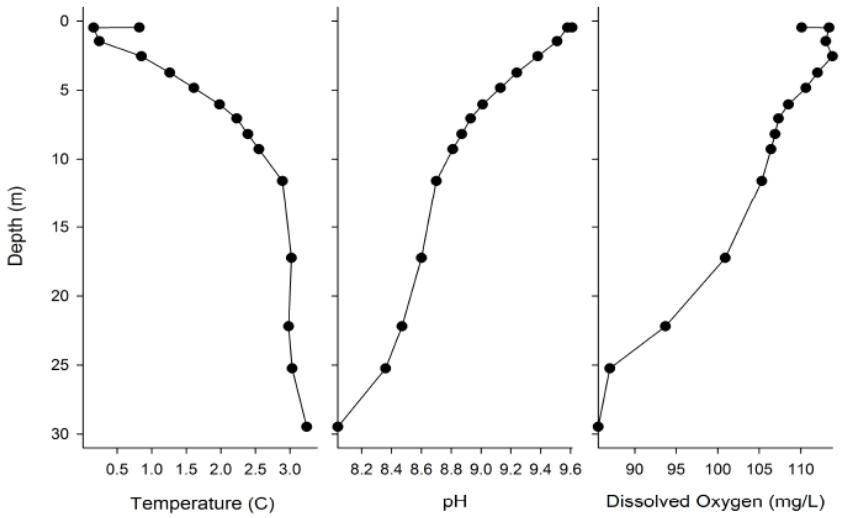

Figure 6. Geochemical data collected at Lower Sermilik on April 10, 2010. Temperature reveals a well-defined thermocline. pH reveals surprisingly basic surface water conditions. Dissolved oxygen content reveals well-oxygenated waters even at depth.

2.3 Sampling and Preparation

Upon return to the United States the sediment cores were split lengthwise, with one half of each section saved for discrete sampling and the other half set aside for archive purposes. Both halves of all sections were then individually wrapped with plastic

sheeting and placed in split-core casings before being transferred to a cold storage facility at the University of Massachusetts Amherst. Discrete sampling was done at 5 cm resolution for all section(s) of each core using stainless steel sampling tools which were cleaned with acetone between samples. All discrete samples were freeze-dried and homogenized in their original glass scintillation vials using a glass stirring rod cleaned with organic solvent prior to all analyses. Samples were then capped and stored for analyses in a cool, dark setting.

2.4 Dating

Chronology for the Lower Sermilik composite core was developed from eight radiocarbon dates, which indicate the composite record extends from 7,700 cal yr BP to present. The radiocarbon dates were made on macrofossils extracted from composite depths of 41.5 cm, 67.5 cm, 91.5 cm, 94 cm, 132 cm, 168 cm, 184 cm, and 229 cm. All radiocarbon ages were calibrated to calendar years using Calib v.6.1 (Stuiver & Reimer, 1993) using the IntCal09 data set (Reimer et al., 2009), and the calibrated ages used are the weighted sum-mean-average of the 2σ ranges (see figure 7). Radiocarbon dates are reported as calendar years prior to 1950 AD (cal yr BP). The chronology for the Lower Sermilik composite core was constructed by applying a smooth spline with a smoothing factor of 0.3 as the weighted average of 10,000 iterations to the age-depth data using the Clam code (Blaauw 2010) for the statistical software “R” (R Development Core Team, 2010). The 95% confidence intervals are calculated by the software as the 2σ range of the mean of the iterations, and are represented as the minimum and maximum ages at each depth. To account for the upper and lower limits of the Lower Sermilik composite core, ages were interpolated from the age-depth model generated.

2.5 Bulk Geochemistry

Using an analytical mass balance, 0.1-70mg of each sample was weighed, and transferred to combusted silver capsules. All discrete samples were analyzed for total organic carbon (%TOC), total nitrogen (%TN), as well as $\delta^{13}C$ and $\delta^{15}N$ of organic carbon on a Thermo Delta V Advantage Isotope Ratio Mass Spectrometer (IRMS) interfaced with a Costech ECS 4010 Elemental Analyzer (EA). Measurements of $\delta^{13}C$ are herein reported relative to VPDB, and measurements of $\delta^{15}N$ are reported relative to AIR.

2.6 Magnetic Susceptibility

Magnetic susceptibility profiles were acquired for all core sections using a GeoTek multi-scan core logger. Magnetic susceptibility was measured at 0.5 cm intervals and the profiles from overlapping depths were used in combination with spectral data, x-radiographs, and physical assessments of sediment to form a composite core from overlapping sections of the A and B cores.

2.7 Slump Identification

Slumped material, herein defined as instantaneous mass-movement deposits (i.e. turbidites), has been removed from the composite core to ensure a more accurate age-depth model. Turbidites in the Lower Sermilik composite core were identified by physical assessment of the sediment cores accompanied by analysis of x-radiograph imagery, magnetic susceptibility data, and elemental profiles. Turbidites were observed to be homogenous in color and consistency with no discernible laminations, occasionally displaying graded bedding. X-radiographs identified the turbidites as zones of low-density relative to the surrounding sediment. The magnetic susceptibility of turbidites is observed to be consistently much higher than in zones of pelagic sedimentation, with

little deviation in these values. Grayscale values obtained using ImageJ® were used on several occasions to help identify smaller turbidites. Grayscale data identified turbidites as elongate intervals of relatively low gray values.

2.8 X-ray fluorescence scanning

High-resolution elemental profiles of each core section were made using an Itrax XRF Core Scanner (Cox Analytical Systems) outfitted with a molybdenum anode. XRF scanning is an advantageous tool as it is non-destructive and is capable of producing extremely high resolution elemental profiles in addition to x-radiograph images, magnetic susceptibility measurements, and digital images**.** For each core, section incremental measurements were taken at 500 micron steps with an exposure time of 20 seconds at a voltage of 50 kv with a current of 45 mA.

2.9 Biogenic Silica

Measurements of Fourier transform infrared spectroscopy (FTIR-S) were conducted in the mid-infrared range on discrete sediment samples for the rapid determination of biogenic silica quantities present in the Lower Sermilik sediment record. Prior to this phase of the analysis, percent-by-weight opal was first determined for 20 discrete samples using a traditional timed digestion-based method (e.g. Mortlock & Froelich 1989; University of Minnesota "Biogenic Silica Analysis Protocol") to provide a calibration dataset. Sediment from the same samples was then mixed with reagent-grade potassium-bromide (KBr) at a ratio of 50:1 (KBr to sediment) and homogenized using a mortar and pestle. KBr is transparent in the IR region and was used as a diluting substance to avoid distortions caused by optical effects (Griffiths & De Haseth 1986; Vogel et al. 2008; Rosen et al. 2010). The samples were then analyzed using a Bruker

Vertex 70 FTIR spectrometer outfitted with a diffuse reflectance accessory (Harrick Inc., USA) for wavelengths between 2,666 and 25,000 nm (3750 to 400cm^{-1}). Prior to the analysis of sediment samples, a 64-count background scan was completed using a sample of ground KBr. This was repeated every 15 samples to account for machine drift. FTIRS spectra of samples were then normalized using a baseline correction to produce the same baseline for all spectra. To assess the relative abundances of opal present in each sample, the area beneath absorbance spectra from 1,050 and 1,250 cm^{-1} was quantified by integration. This area was chosen due to the characteristic SiO absorbance maxima observed at 1,100 cm^{-1} associated with opal (Moenke 1974; Gendron-Badou et al. 2003; Vogel et al. 2008; Rosen et al. 2010).

Partial least squares regression (PLS) (e.g. Martens and Næs 1989) was used to develop a transfer function between the FTIRS spectra of the sediment and measured values of BSi (e.g. Rosen et al. 2010). All measured BSi values were square root transformed prior to analysis in order to normalize the data distribution (Vogel et al. 2008; Rosen et al. 2010). The number of significant components for the PLS was assessed by a leave-one-out style of cross-validation (CV) the SIMPLS algorithm (de Jong, 1993). Cross validation is critical step when fitting models to be used for prediction, and is used to estimate the expected level of fit of a model to a data set, independent of the data that were used to train the model. Leave-one-out cross-validation employs a single observation from the original sample as the validation data, and the remaining observations as the training data. This is repeated such that each observation in the sample is used once as the validation data.

The relationship between the FTIRS spectra and the corresponding BSi values shows a statistically significant correlation. A 1-component PLS model gives an R^2_{CV} = 0.75 and root mean square error of prediction (RMSEP) = |0.37|.

CHAPTER 3

RESULTS

As we rush forward into the future, the body of evidence in support of climate change grows (Kaufman 2009), forcing us to ask new and challenging questions. At the forefront of these is the pervasive question of how Earth's climate system has changed in the past. This question is the backbone of paleoclimatology, and the principal means of determining how the Earth will respond to anthropogenic forcings. From decades of geological research, a shadowy outline of Earth's climatic history has emerged from studies of individual records, but the spatiotemporal resolution of these records is limited. To glean a full understanding of the dynamic processes that influence climate a network of climate records must be established around the globe. From this network we can examine trends with more confidence, explore teleconnections, and both large and small scale variability may be disentangled.

The Lower Sermilik record provides a unique opportunity to study Holocene climate change in a Low Arctic setting due to its proximity to the Greenland Ice Sheet, the North Atlantic Ocean, and two nearby meteorological stations. It also benefits from previous studies which have explored the nearby Mittivvakkat Glacier (e.g. Humlum et al. 2008), bedrock geology (e.g. Bridgewater 1974), and other lake studies from the eastern and western coasts of Greenland.

3.1 Chronology

A total of 8 AMS radiocarbon dates were used to construct the chronology of the Lower Sermilik composite core. Dating was done at the Keck Carbon Cycle AMS Facility at the University of California Irvine. The samples of macroscopic vegetation were collected at successive depths. Two additional dates were initially recovered in 2010, however these remains were each located within a zone later identified as a

turbidite, and exhibited an age-reversal. The oldest calibrated age was collected from a depth of 229 centimeters down core, which returned a date between 5996 and 6180 cal yr BP (95% confidence). Unfortunately no macroscopic remains of vegetation were located closer to the transitional boundary between the glacio-fluvial environment of Unit I and the stable lake environment of unit II, thus leaving the timing of this transition to the interpolation of the age-depth model (see figure 7).

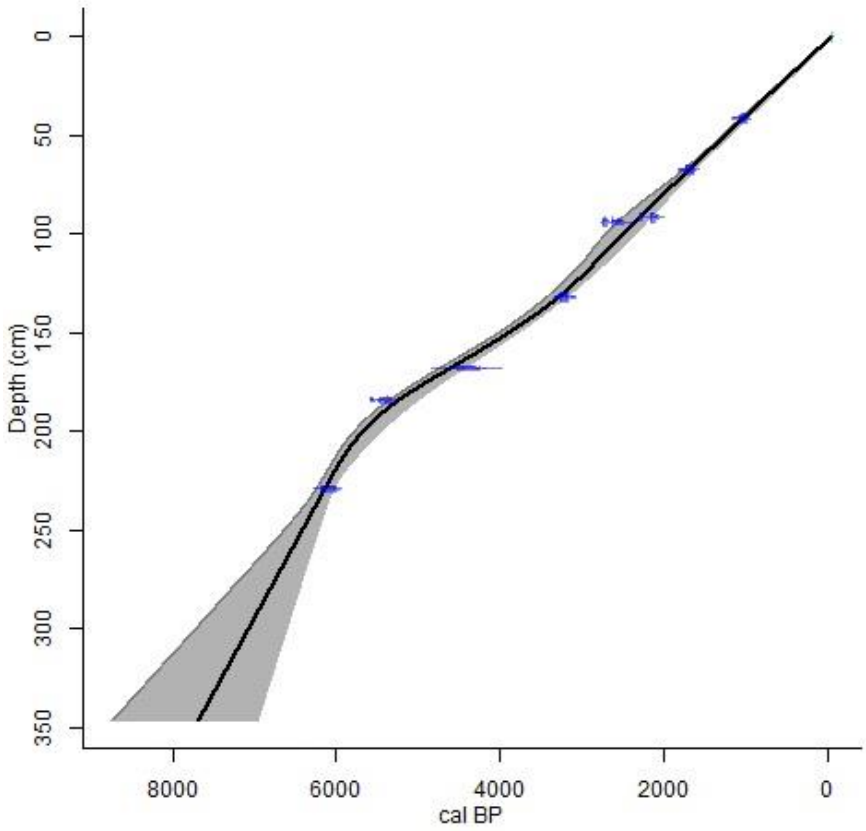

Figure 7. Lower Sermilik interpolated chronology made using Clam for the open source program R. Blue points represent AMS radiocarbon dates, and are spread to include the statistical age-range returned for each date. The gray shading indicates the 2 sigma 95% confidence envelope.

3.1.2 Turbidite removal

A total of 23 turbidites were removed from the Lower Sermilik composite core. The size of these turbidites is highly variable, ranging from sub-centimeter scale to tens of centimeters. The removal of these zones of instantaneous deposition resulted in a more accurate age-depth model. Identification was made using visual inspection, elemental profiles, and magnetic susceptibility data **(**Figure 8**)**. The total amount of sediment removed from the composite core in form of turbidites is 138 cm.

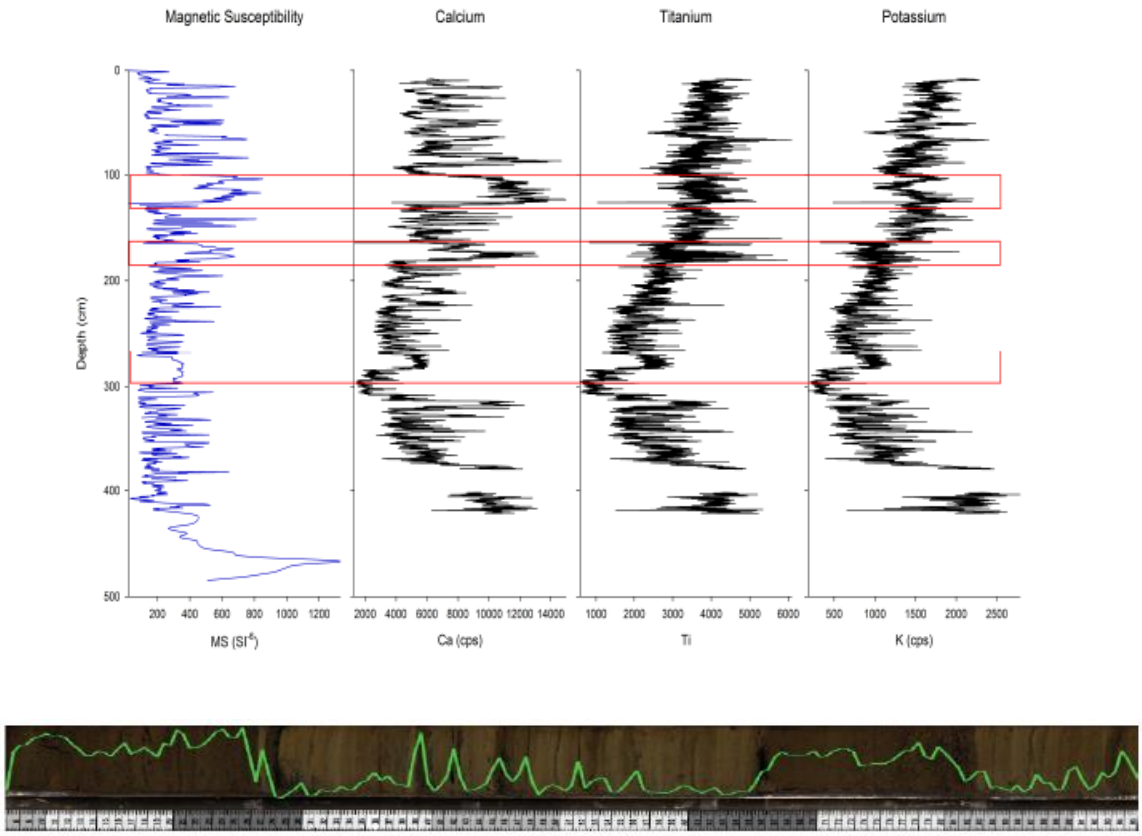

Figure 8. Identification of turbidites. Above: Turbidite identification using magnetic susceptibility and elemental profiles. Highlighted by red boxes are the three largest turbidites as an example. Below: Example of the identification of two major and several minor turbidites using magnetic susceptibility profiles coupled with visual inspection.

3.2 Core lithology

The Lower Sermilik record consists of three distinct sediment units: a coarse-grained, minerogenic unit (Unit I), a finely-laminated and organic-rich unit (Unit II), and a lighter-colored, coarsely-laminated unit (Unit III). Each of these units is indicative of the depositional environment in which it was formed.

3.2.1 Unit I

Unit I extends from the bottom of the composite core (346 cm) to 284 cm. The base of Unit I is composed of clast-supported glacial debris intermixed with coarse, siliceous sand. Above this portion of the unit are fine, sandy laminations that become finer and more well-defined up-core. Laminations above 306 centimeters in Unit I are highly disturbed, exhibiting evidence of turbid depositional conditions or events. This unit is characterized by unusually high magnetic susceptibility, and contains heightened XRF counts of alkali metals, alkaline earth metals, transition metals, and metalloids (e.g. K, Rb, Ca, Sr, Mn, Ti, Mn, Fe, Ni, Si) (see figure 9). No datable organic material was recovered from Unit I, but the extrapolated age of the base is approximately 7,800 cal yr BP.

Unit I is interpreted to represent a depositional environment immediately following local deglaciation, as Lower Sermilik emerged from beneath the ice. The presence of clasts (up to 5 cm) indicates a high-energy environment, which was likely supplied by proximal melting ice. The coarse sand, devoid of organic material, also strongly suggests a time when the lake basin had emerged from beneath perennial ice but depositional processes were still strongly influenced by the glacier.

3.2.2 Unit II

Unit II extends from 283 centimeters to 140 centimeters. The base of Unit II is finely laminated with good preservation and an abundance of organic matter. There is a striking disparity between lamination colors, perhaps owing to different proportions in organic and mineral content. Up core, the laminations of Unit II thicken slightly, and there are several notable turbidites present, though there is no apparent periodicity to the appearance of turbidites. The composition of this unit is markedly different from Unit I and is composed of clay, silt, and fine sand with abundant organic material. Much variability is noted in the elemental composition of this unit, with intriguing sinusoidal patterns seen in elements associated the underlying bedrock (e.g. Ti, K, Rb) (see figure 9), which may be attributable to atmospheric oscillations or periodic ocean events associated with precipitation anomalies (see figure 9). Three samples for AMS radiocarbon dates were collected within this unit, and the upper and lower interpolated bounds of this unit are 3367 and 6900 cal yr BP respectively (see figure 7).

Unit II is interpreted to represent a depositional environment from the Holocene Climatic Optimum as experienced in Southeast Greenland. This is supported by the abundance of organics present in this unit of the composite core, and the dearth of glacially-influenced sediment deposits (see figure 10). One interesting feature noted in this core is the appearance of what have been interpreted as avalanche deposits. These deposits are much coarser than is typical for other turbidites, though there is also grading of these deposits.

3.2.3 Unit III

Unit III extends from 139 centimeters to the top of the composite core. Unit III is characterized by more robust laminations with little color variability in comparison to

Unit II. Due to the homogenous color of Unit III differences between laminations are occasionally visible in x-radiograph images. This unit begins with steadily increasing concentrations of alkali metals, alkaline earth metals, transition metals, and metalloids reminiscent of Unit I (see figure 9). Unusually high levels of organic matter are noted in this unit, perhaps due to increased catchment erosion due to destabilization, nutrient availability, or bottom water conditions conducive to preserving organic matter. AMS radiocarbon dates were evaluated from five macroscopic samples of organic material, giving maximum and minimum age boundaries of 3367 and -60 cal yr BP respectively for this unit.

Unit III is interpreted to represent a depositional environment reflecting the effects of neoglaciation. A characteristic of this is the high level of elements associated with erosion. The most fascinating aspect of this unit, however, is the surprising abundance of organic matter at a time associated with cooling.

3.3 Biogenic Silica

Biogenic silica (BSi), composed of hydrated silicon hydroxide, is primarily produced by diatoms and is used to form the characteristic rigid diatom cell wall known as a frustule. Diatoms are unicellular, photosynthetic algae found in a wide range of environments, including lakes. When diatoms die, their dense frustules sink to the bottom of bodies of water and are incorporated into sediments as biogenic silica microfossils. The abundance of biogenic silica in sediments can be used to infer the relative past populations of diatoms, and is thus an excellent proxy for paleolimnologists seeking to reconstruct measures of paleo-productivity (Conley 1988).

Discrete sediment samples were collected at 1 centimeter resolution from 0 to 17.5 centimeters and at 5 centimeter resolution from 18 to 314 centimeters. These samples were combined with potassium-bromide at a ratio of 50:1 (Kbr:sediment) and were analyzed using a Bruker Vertex 70 FTIR spectrometer outfitted with a diffuse reflectance accessory (Harrick, Inc., USA). The area under the resultant chromatogram peak from 1,000 to 1,250 reciprocal centimeters was integrated and quantified into percent biogenic opal using a one-component partial least squares regression.

Findings reveal small concentrations (<5%) of biogenic opal in the Lower Sermilik sediment record as early as 7300 cal years BP, suggesting a sparse population of diatoms present in Lower Sermilik shortly after local deglaciation (see Figure 10). From 7300 through 6900 cal yr BP the abundance of biogenic silica declined sharply to a minimum of less than 1%. From this minimum value, concentrations of biogenic opal rose extremely rapidly and consistently from 6900 cal yr BP, reaching a middle-Holocene maximum of 25% by 6200 cal yr BP. With the exception of a negative excursion at 6050 cal yr BP, biogenic opal concentrations remained consistently high with little variability until 3200 cal yr BP, though a negative trend in biogenic opal is observed to begin approximately 1000 years earlier. This period of large, sustained diatom populations is likely due to the local expression of the Holocene climatic Optimum, a period of relative warmth and climate stability (Marcott et al 2013). The drop observed in the diatom population at 3200 cal yr BP marks the transition from a warm, stable climate into neoglaciation, and coincides approximately with the reappearance of the Mittivakkat Glacier proximally located to the Northwest of Lower Sermilik. From 3200 cal yr BP until 1240 cal yr BP concentrations of biogenic silica remained comparably low and

exhibit high, saw tooth-like variability. Around 1240 cal yr BP percent biogenic opal began to trend positively, with a noteworthy period of stability from 1220 cal yr BP until 400 cal yr BP. Though this period of time exceeds the total duration of the Medieval Climate Anomaly (MCA), it is not unreasonable to consider that some of this stabilization and population growth may have been in part a response to the MCA. Starting at 390 cal yr BP the concentration of biogenic opal dropped dramatically from 20% to 2% at 320 cal yr BP, and did not recover to MCA levels until 227 cal yr BP. From this point onward biogenic opal concentrations rose steadily and sharply through the post-industrial era, reaching a Holocene maximum of 26% in the top centimeter of the Lower Sermilik composite core.

The trends observed in the biogenic opal record, reflecting diatom populations and preservation of diatom tests are interpreted to represent primary productivity in Lower Sermilik. It is notable that the trend of biogenic opal closely mirrors that of Holocene temperature trends (Wagner et al., 2000).

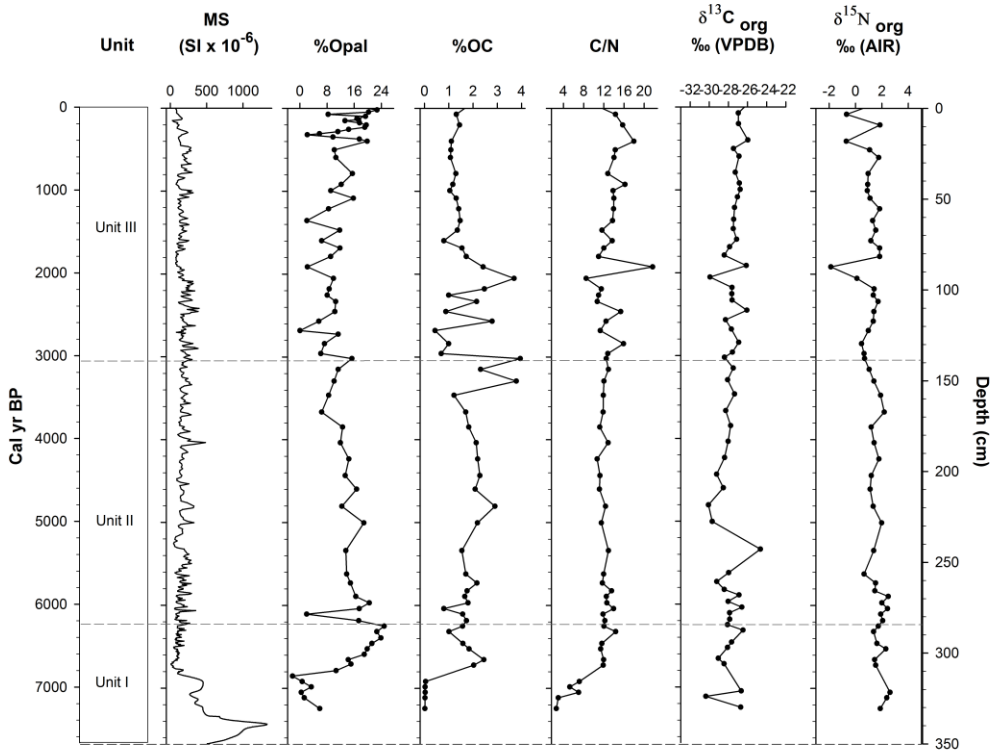

Figure 9. Bulk geochemical data for the Lower Sermilik composite core plotted against age. Dashed lines represent major transitions in the core based on changes in lithology. Unit I is characterized by cobbles, sand, and clay. Unit II is characterized by fine, dark, organic-rich laminations. Unit III is homogenous in color and exhibits laminations thicker than those observed in Unit II.

3.4 Bulk Geochemistry

3.4.1 Organic Carbon

The percentage of organic carbon (%OC) present in lacustrine sediments is a useful and straightforward proxy for identifying the amount of organic matter in sediments. Though sometimes viewed as a rough proxy for autochthonous and allochthonous productivity, %OC should be viewed simply as the amount of organic matter preserved in sediments (e.g. Meyers 1993; Meyers 1997; Meyers 2003). There are

complex controls on the %OC preserved in sediments, including rates of degradation and diagenesis, transport of terrestrial organic matter into the lake from the catchment, and microbial and algal contributions of organic matter.

Percent organic carbon in the Lower Sermilik sediment record was measured in discrete samples using a Costech ECS 4010 Elemental Analyzer at 5 cm resolution from 0 to 314 centimeters in the Lower Sermilik composite core (see Figure 10). No measurements were made below this depth due to the presence of only coarse sand and cobbles. Measurements of organic carbon starting 7300 yr BP (314 cm depth) reveal no notable presence of organic carbon, with values not exceeding 0.05% OC until 6750 cal yr BP when %OC jumped to 2% and to 2.5% by 6680 cal yr BP. Values of OC for the period immediately following deglaciation rapidly fell to stable mean values of about 1.5%. The initial spike seen in organic carbon in the Lower Sermilik sediment record may reflect increased algal productivity as the combined result of warming temperatures consistent with Holocene trends and large-influxes of nutrients into the lake from the not-yet-stabilized catchment. The catchment at this time would have likely received substantial groundwater flow from the retreating valley glacier, and because the landscape had recently been glacially-eroded there would not have been much topsoil for terrestrial post-glacial vegetation to set deep root systems. Melt water from the valley glacier during summer months, in addition to the seasonal melting of the snow pack, would have been able to transport larger amounts of clays rich in phosphorus as well as nitrogen in the form of dead terrestrial vegetation.

From 6450 cal yr BP until 3680 cal yr BP %OC remained for the most part stable and with comparably high values, although a negative trend is apparent starting after

4590 cal yr BP. This period of high and stable percentages of organic carbon most likely reflect the local occurrence of the Holocene Climatic Optimum, and the negative trend seen from 4590 to 3380 cal yr BP marks the decline into neoglaciation. Interestingly, %OC preserved in the Lower Sermilik composite core records a series of major positive excursions between 3380 and 1692 cal yr BP. Though these data contradict the expectation of decreased vegetation during neoglacial conditions, further examination of the history of Ammassalik Island provides several possible explanations. At approximately the same time the Mittivakkat Glacier is estimated to have formed directly to the Northwest of Lower Sermilik. This date is based on the beryllium-10 dating of Mittivakkat moraines conducted by Humlum et al., 2008 as part of a geomorphological study of Ammassalik Island funded by the Danish Geological Survey. The appearance of a major land-based glacier would have led to increased weathering and erosion of bedrock material, resulting in increased production and transport of phosphorus-bearing clays. In modern lake systems phosphorus is commonly cited as the primary limiting-factor of algal productivity. In an oligotrophic lake system such as Lower Sermilik a sharp rise in available nutrients could conceivably result in increased productivity despite cooling temperatures. There also exists the possibility of prolonged seasonal ice cover of Lower Sermilik due to steadily cooling temperatures. This could have resulted in a reduced oxygen supply to the lake and therefore resulting in suboxic to anoxic bottom water conditions, ideal for preserving organic matter. There is also the possibility of catchment destabilization, simply resulting in more organic matter being transported into Lower Sermilik via groundwater flow.

The major positive excursions in %OC ceased by 1530 cal yr BP and from 1470 until 400 cal yr BP %OC remains exceptionally stable, remaining at values very close to 1%. After 400 cal yr BP %OC steadily increased, ending at 1.8% in the top 1 cm of the Lower Sermilik composite core. The major trends seen in %OC do not seem to follow the trends seen in Holocene temperature reconstructions, and instead seem to more likely reflect the stability of the Lower Sermilik catchment and controls on erosional transport.

3.4.2 C/N ratio

The ratio of total organic carbon to total nitrogen (C_{org}/N_{total}) is a useful tool for identifying the proportions of algal and land-plant organic matter (Kaushal and Bindford 1999; Meyers 1993). Modern organic matter from algae, which contain a high ratio of protein to cellulose, commonly produces C/N values between 4 and 10. Conversely, modern organic matter derived from vascular land plants, which have a high ratio of cellulose to proteins, commonly have C/N values of 20 and greater (Meyers 1993).

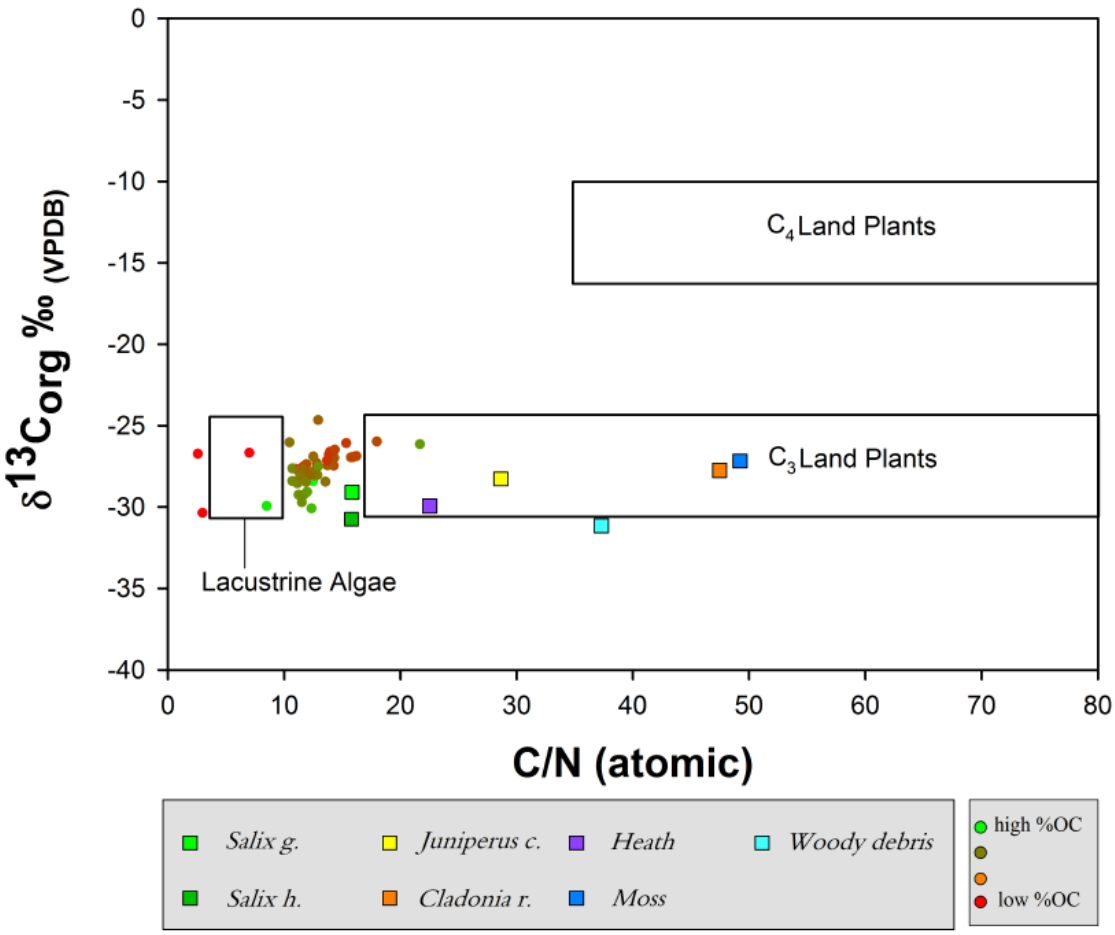

Figure 10. Paired carbon isotopic values and atomically corrected C/N values for discrete sediment samples. Individual samples plotted as circles are graded from red to green based on the % organic carbon of each sample. Modern vegetation data from samples collected at the Lower Sermilik catchment are plotted as color-coded squares.

The C/N values measured in the Lower Sermilik sediment record remain extremely stable throughout the Holocene (Figure 10). Prior to 6900 cal yr BP C/N remained very low as a result of nitrogen being relatively more abundant than organic carbon, though (compared to later) nitrogen was also very limited during this period. This level of background nitrogen is likely to be inorganic in origin, though occurring in quantities so small (<0.001%) that correcting the C/N ratio to account for it is

unnecessary. Shortly after transitioning from the post-glacial sediments of Unit I at 6900 cal yr BP, the ratio of C/N assumed extremely constant values rarely fluctuating outside of a range between 9.5 and 12. These values are higher than expected for a purely algal or autochthonous source and markedly lower than C/N values indicative of a purely terrestrial source. It is of importance to note, however, that modern samples of *Salix herbacea* and *Salix glauca* collected from within the Lower Sermilik catchment produced C/N values of 13.5. Though these dwarf willow species were abundant in the catchment, it seems unlikely that they are the primary supplier of organic matter into Lower Sermilik. These findings suggest that the majority of organic matter preserved in the Lower Sermilik sediment record is from autochthonous sources, although a secondary source of organic matter from the terrestrial realm seems likely.

The period of marked stability beginning at 6900 cal yr BP terminated at 3000 cal yr BP. From 3000 cal yr BP until 360 cal yr BP C/N values experienced high variability superimposed upon a long-term positive trend, with numerous positive swings occurring around the onset of Unit III. From 360 cal yr BP until the top of the sediment record C/N values dropped significantly, terminating at a value of <9. This suggests that since the onset of the Little Ice Age the dominant source of organic matter in Lower Sermilik is algal.

3.4.3 $\delta^{13}C_{organic}$

The carbon isotopic composition of organic matter derived from lake sediments can be used as a proxy for identifying contributions of C_3 plants, C_4 plants, and algae to organic matter (e.g. Talbot and Johannessen 1992; Hodell and Schelske 1998), as well as for inferring nutrient availability. Unfortunately the dissolved CO_2 produced by lacustrine

phytoplankton is typically in equilibrium with the atmosphere, making contributions of organic material from lacustrine algal sources indistinguishable from vascular plant contributions (Meyers 1997).

The carbon isotopic composition of organic matter in Lower Sermilik shows high variability within the small confines of -30‰ to -25‰ (Figure 10). This range of values is consistent with $\delta^{13}C_{org}$ ‰ values of lacustrine algae and C_3 plants. This comes as no surprise for Lower Sermilik, and merely confirms the assumption inferred from the Lower Sermilik C/N ratio that algal production is likely the primary source of organic material, and that input of vascular plant debris from the catchment is a secondary source. In Units I and II there is high variability between sampling intervals superimposed on a trend of depletion. This relationship is reversed in Unit III as values reflect generally lower variability and follow a long term enriching trend through the top of the core. The variation noted may reflect small source changes or perhaps nutrient availability related to the influx of soil enriched in dissolved inorganic carbon.

3.4.4 $\delta^{15}N_{total}$

The nitrogen isotopic composition of sediments derived from lakes can sometimes aid in the identification of sources of organic matter based upon the difference between the $^{15}N/^{14}N$ ratios available in terrestrial reservoirs versus aquatic reservoirs (e.g. Talbot 2002; Meyers 2003). Nitrate, which is the most common form of dissolved inorganic nitrogen used by algae, typically has $\delta^{15}N$ values of 7-10‰, while atmosphere-derived nitrogen available to land plants has values close to 0.5‰. C_3 land plants (Peterson and Howarth 1987, Meyers 2003). There are, however, complicating factors that must be taken into consideration when making ecological interpretations based on $\delta^{15}N$. For

instance, low values can also be attributed to biological nitrogen fixation which occurs when atmospheric nitrogen is converted to ammonia by the enzyme nitrogenase. The conversion of nitrogen to ammonia can be attributed to many organisms, but very frequently the culprit organisms are cyanobacteria (blue-green algae) (Fogel and Cifuentes 1993).

The values of $\delta^{15}N$ in the Lower Sermilik sediment record range from -1.86 to +2.48 with significant excursions coincident with those of the Lower Sermilik $\delta^{13}C$ record (Figure 10). The most noteworthy excursion seen in the $\delta^{15}N$ record occurs at 76.5 cm and reaches a value of -1.86. This excursion shares timing with a large relative enrichment of $\delta^{13}C$, a rise in C/N values, and a major peak of %OC. The timing of this event coincides with a period of suboxic to anoxic conditions inferred from the ratio of Mn/Fe at this depth. The values of this signal suggest a terrestrial source of nitrogen; however values of C/N indicate that terrestrial sources may play a secondary role to aquatic sources of organic matter. If this is indeed the case then there is a strong likelihood that nitrogen fixation occurred in Lower Sermilik throughout the Holocene.

3.5 X-ray fluorescence scanning

Elemental profiles in the sediments of remote lakes offer an opportunity to consider the impacts of natural events on depositional processes and on conditions at the sediment-water interface. Major controls on the elemental makeup of sediments recorded in Lower Sermilik include physical processes and changes in redox conditions due to biological activity. Major, trace, and mobile elements within sediment sequences (as well as sediment properties such as %OC, grain size, and %opal) reflect these conditions and provide a means of reconstructing paleo-depositional environments.

All elemental profiles for this study were made using a COX Analytical ITrax X-Ray fluorescence core scanner**.** Values are reported in counts per second (CPS), and are not intended to be interpreted as absolute values or absolute concentrations. These values are, however, useful for noting the relative distribution of various elements throughout the length of the core.

The majority of the elemental profiles generated from the Lower Sermilik core reflect extremely similar trends, suggesting that the transport of materials into the lake is controlled by a primary mode acting as the driving force behind all elemental inclusions. Although the overarching trends of most elements appear similar, few share statistically significant relationships.

3.5.1 Alkali Metals: Ca, Sr, Ba

Alkali metals calcium, strontium, and barium are all present in the Lower Sermilik sediment record and exhibit significant counts per second (>200 cps). Calcium and strontium share a statistically significant relationship (R^2=0.75) and it isvery likely both source from the abundant orthopyroxines found in the basic charnockite complex which underlies the catchment of Lower Sermilik. Barium does not share a statistically significant relationship with either (R^2=0.20, 0.21 respectively), suggesting barium sources are different than calcium and strontium. The hypothesis that Sr and Ca sources are different than Ba is further supported by the extremely high variability seen in Ba,unlike Ca and Sr, which share common peaks and exhibit nearly identical behavior (Figure 9). It is also worth noting that the counts per second recorded for Ca and Sr typically exceed that of Ba by an order of magnitude.

3.5.2 Alkaline Earth Metals: K, Rb

Alkaline metals potassium and rubidium are both found in the Lower Sermilik core in abundance. The relationship between the two elements is not statistically significant suggesting separate sources (R^2=0.32). The small relationship reported by this R^2 value reflects merely that during periods of enhanced transport both increase and likewise during periods of decreased transport the abundance of each element diminishes (Figure 9). The strongest relationship potassium shares with another element is with titanium, exhibiting an R^2 value of 0.83.

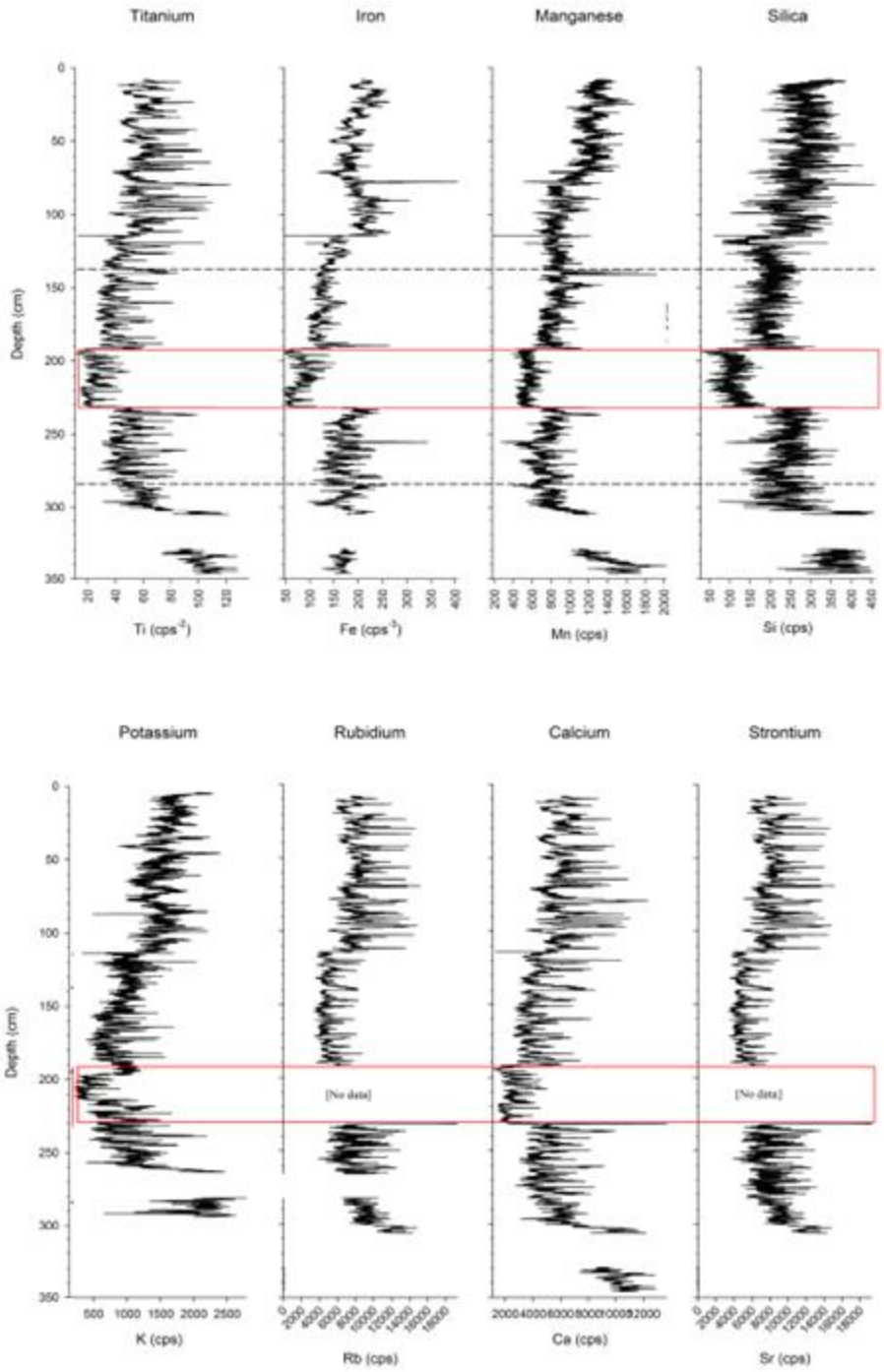

Figure 11. XRF counts of major elements in the Lower Sermilik composite core. The zone highlighted in red was scanned at a later data than other sections and the absolute values from this section are dubious

3.5.3 Transition Metals & Metalloids

3.5.3.1 Titanium

High-grade metamorphic rocks with intrusive igneous origins, like the bedrock of Ammassalik Island, frequently contain quantities of titanium. Weathering and erosion of Ti-rich rocks and sediments is thought to be the primary source of titanium in Lower Sermilik. Initially incorporated into the high-grade metamorphic rocks of this area, titanium would have entered the lake primarily through groundwater or fuvial processes, though also undoubtedly some has entered the lake via eolian transport as well. For this reason titanium is deemed to be indicative of weathering conditions, with increased quantities representing increased weathering and transport.

Titanium in the Lower Sermilik core is extremely abundant and exhibits high variability superimposed upon lower frequency trends. The highest values are noted near the base of Unit I, which quickly drop to mean levels around the onset of Unit II. In portions of Unit II an apparent periodicity is noted at 6.5 to 9 cm intervals (90-130 cal years). The transition into Unit I is marked by an increased baseline of titanium values along with more consistently large peaks superimposed upon it.

3.5.3.2 Manganese

Manganese in the Lower Sermilik core is highly abundant, exhibiting up to 2000 counts per second near at the base of Unit I. These values quickly drop off and settle around 700 cps for most of unit II. A sharp rise is noted at the end of Unit II, quickly falling to lower values at the onset of Unit I. Values recover to Unit II levels by 1840 cal yr BP (75 cm) and continue to increase until reaching a relatively stable baseline of ~1200 cps for the final 1740 (70 cm) of Unit I.

3.5.3.3 Iron

Iron is an unusual element in the Lower Sermilik sediment record. Iron is the most abundant element in terms of counts detected during XRF scanning. Unlike other elements, iron is not exceptionally abundant in the glacio-fluvial basal debris of Unit I. In the basal debris of Unit I values begin at 18,000 cps and rapidly fall to a minimum of 6,000 cps before rapidly increasing back to mean values of 17,000 cps at the onset of Unit II. Values experience great variability in Unit II, though these excursions are not superimposed on any larger-scale trends. Starting at 5400 cal yr BP (184 cm) values drop to a mean baseline of around 12,500 and remain at this level until 2900 cal yr BP (112 cm) cm, at which point values rapidly jump up to 26,000 cps. From 2900 cal yr BP (112 cm) onward values remain relatively high though a negative trend is seen until 1600 cal yr BP (64 cm), at which point the trend reverses to slightly positive.

3.5.3.4 Silica

In this study silica displays the trend common to most elements in the Lower Sermilik sediment record with high variability superimposed on large-scale trends. Values are greatest in the basal debris of Unit I, but rapidly decline before recovering rapidly at the onset of Unit II. Unit II begins with nearly mean values, but exhibits a short negative trend until 142 cm (date) before recovering to stable values. At the transitional boundaries of Unit II and Unit I silica values experience a sharp decline before rapidly recovering at 114 cm (~date). From this point onward silica values remain generally high but continuously variable until reaching consistently high values in the final centimeters of Unit I. Undoubtedly the silica found in Lower Sermilik has many sources, including the basic charnockite complex underlying Lower Sermilik, the granite gneiss complex to

the North of Lower Sermilik, soils, glacial debris, and from distal sources via eolian transport.

3.5.4 Elemental Ratios

3.5.4.1 Mn/Fe ratio

The ratio of manganese to iron in lake sediments is commonly used as an indicator of redox conditions at the sediment-water interface at the time of deposition. Low values correspond to periods of suboxic or anoxic conditions (Chirinos et al. 2005). The values observed in the Lower Sermilik sediment record reveal high frequency variations superimposed on large-scale trends (Figure 12).

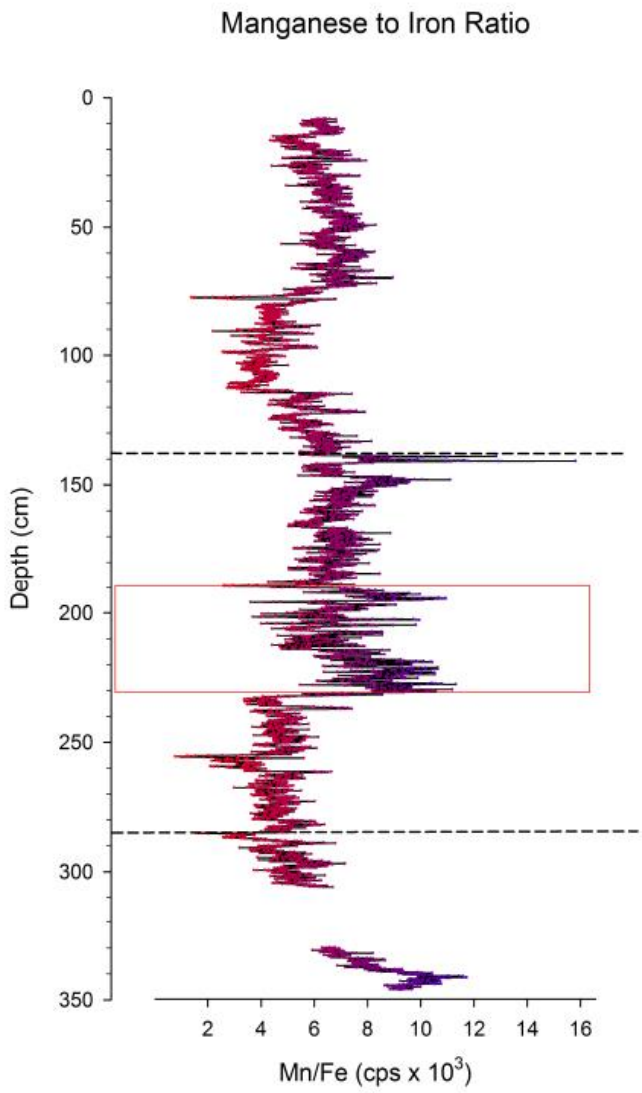

Figure 12. The ratio of counts of manganese to iron measured in the Lower Sermilik composite core. Lower values are associated with sub-oxic conditions at the sediment-water interface. The zone highlighted by the red box indicates a core section scanned at a later date and which returned absolute values not concurrent with the rest of the core. Dashed lines indicate transitions seen in core lithology.

The data for the ratio of manganese to iron (counts) in Unit I is severely limited due to invalid readings identified by the XRF scanner, however the available data

reveal a negative trend from 305 centimeters to the boundary of Unit I and unit II at 284 centimeters (see figure 11).

Unit two shows an immediate recovery from the negative trend observed in Unit I and returns to mean values of ~0.0045 from 284 cm to 261 cm. This stability is lost in an abrupt negative excursion from 261 cm through 254 cm, at which point the mean values rapidly recover to values similar to those seen at the beginning of Unit II. From 232 cm through 190 cm no data are available due to invalid readings from the XRF scanner. Interpolation between these points suggests slowly rising values, which is inferred by a positive trend that began after this gap. This positive trend continues until 146 cm, followed by a brief and abrupt negative excursion, immediately followed by an abrupt but brief positive excursion at the boundaries of Unit II and Unit III at 139 cm (Figure 11).

Mn/Fe values show a major negative excursion beginning at the onset of Unit III. This negative excursion continues from 138 cm through 73 cm, reaching a minimum value of ~0.001 at 73 cm. This excursion coincides with the major positive excursions seen in %OC, C/N, $\delta^{15}N$, and $\delta^{13}C$. Beginning around 73 cm values return to normal, but rapidly reveal a gradual negative trend.

3.5.4.2 Si/K ratio

The ratio of silica to potassium reveals a fascinating history of the Lower Sermilik catchment. Ammassalik Island is subject to strong, persistent northeasterly winds, which over the course of thousands of years have formed dunes on the island (Humlum et al., 2008). Though silica incorporated into Lower Sermilik Lake is thought to represent a

primarily terrestrial signal, a large portion of silica is likely transported into Lower Sermilik via eolian processes.

Periods of time when the potassium-rich rocks of the Lower Sermilik catchment are being mechanically weathered (e.g. deglaciation, neoglaciation) coincide with periods of low silica to potassium ratios. During stable periods (e.g. the Holocene Climatic Optimum) the large influxes of potassium ceased, along with a similar trend seen in most major elements measured in the Lower Sermilik core. During periods of arguably lower intensities of mechanical weathering the ratio of silica to potassium rises notably, and the signal becomes much more variable. It seems that when there is not an overprint of secondary transport signals (e.g. intense precipitation or melting events or periods of increased eolian transport or intense glacial erosion) distinct periods become apparent. The best example of this in the Lower Sermilik core occurs between 276 and 222 centimeters (Figure 14), when a clear 90-130 year signal is very strong (Figure 13, Figure 14). During these periods the ratio of silica to potassium experiences intense variability over very short timescales. Similar peaks are observed throughout Unit II further up core, however the signal is not quite as strong, nor does it occur with such striking periodicity. Though the origin of this variability is not certain, it does function on timescales similar to that of large-scale AMO shifts. It is though that these periodic, secondary signals do indeed exist throughout much of the Lower Sermilik core, however they are overwhelmed by overall sediment input except for periods of exceptional stability.

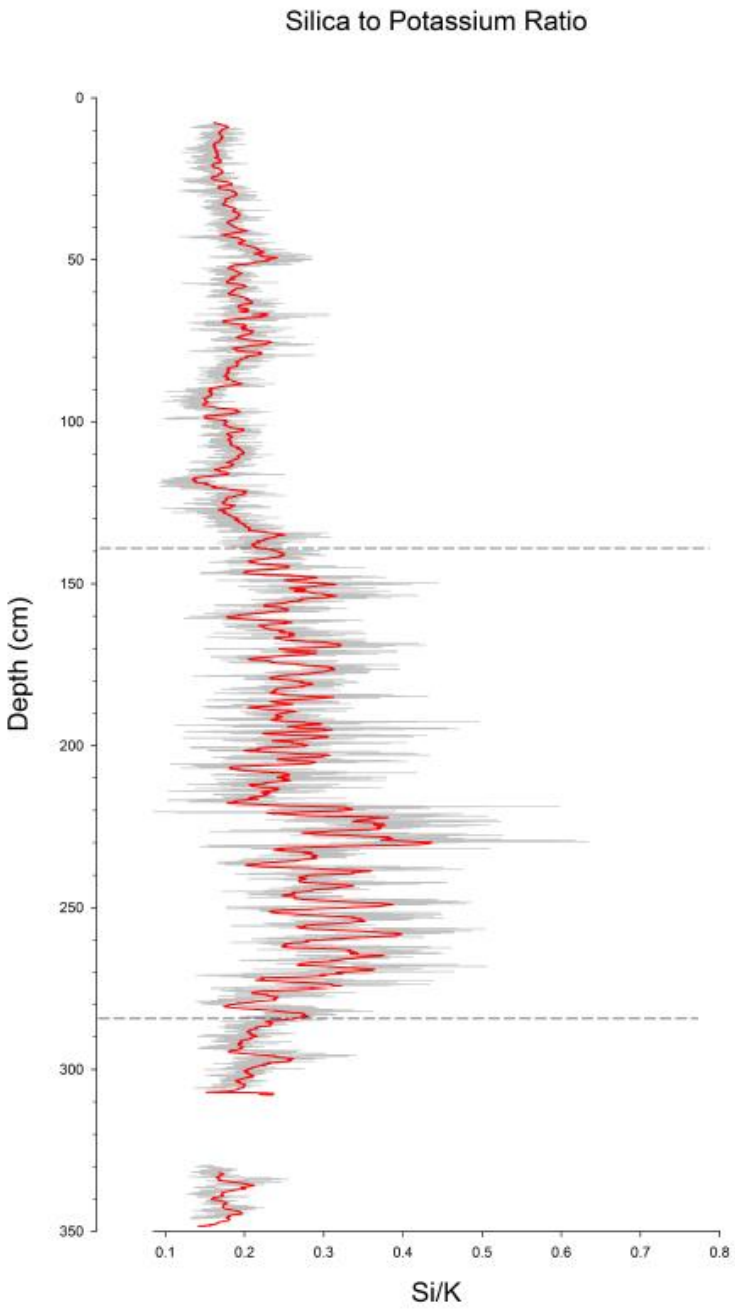

Figure 13. The ratio of silica to potassium in the Lower Sermilik composite core. Lower values are interpreted to be associated with potassium-rich clays, which would indicate a greater amount of mechanical weathering of bedrock taking place in or near the catchment. The zone from 276-222 (6800-6050 cal yr BP) centimeters shows a strong 90-130 year periodicity (Figure 14), suggesting an oscillating environmental signal.

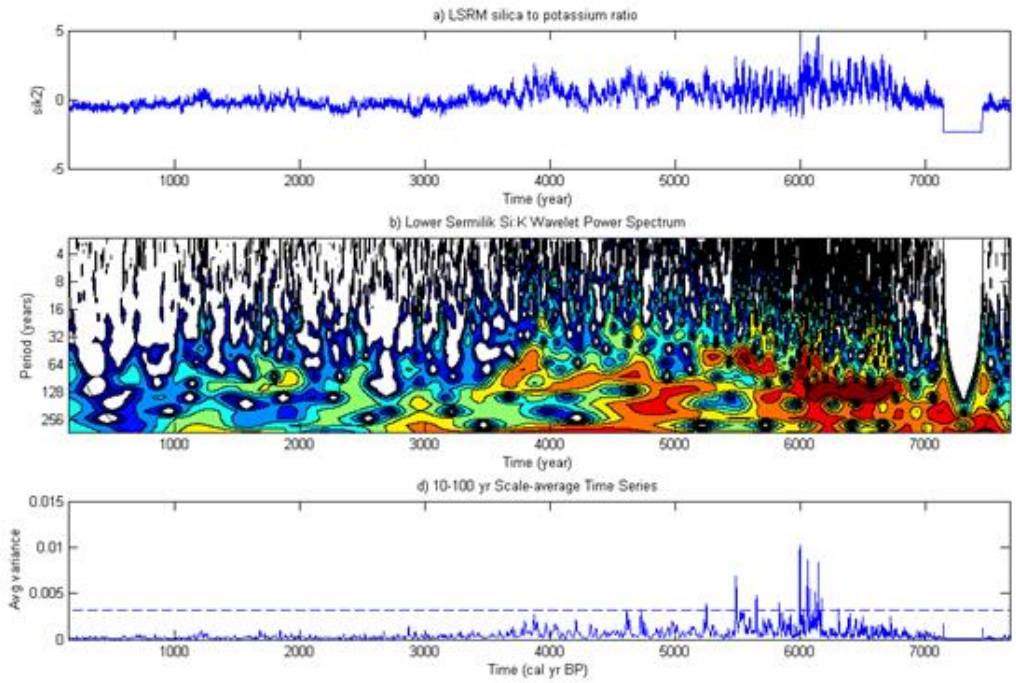

Figure 14. Wavelet analysis of the Lower Sermilik Silica to potassium ratio. Top: The ratio of silica to potassium throughout the entire composite core. Middle: Power diagram exhibiting a high level of variability occurring at a period of 90-130 years from 6800 to 6050 cal yr BP. Bottom: Average variance seen throughout the composite core.

Unit I exhibits relatively low ratios of silica to potassium, indicating a dominant source of potassium from freshly eroded material provided by the receding valley glacier. Several excursions of proportionally-higher silica values correspond to exceptionally sandy zones.

Unit II exhibits highly variably ratios of silica to potassium, with peaks exhibiting apparent periodicity from 276 cm to 222 cm, and then again at a slightly higher frequency from 212 through 167 cm. These peaks of proportionally higher amounts of silica to potassium occur roughly 6 cm apart, which correspond to a period of approximately 90 years. This relationship holds for the zone between 212 and 167 centimeters, though the strength of the signal is somewhat weaker. Overall Unit II displays strongly positive

values of Si/K, suggesting perhaps a highly stabilized catchment or decreased strength of transport within the catchment.

Unit III exhibits much lower values of Si/K than is seen in Unit II, and strongly resembles the values observed in unit I. The lowest values of Si/K are measured from 134 cm to 82 cm, which indicates strong transport of materials from the catchment, perhaps as the result of more proximal ice due to the onset of neoglaciation.

CHAPTER 4

DISCUSSION

4.1 Organic Matter

The percent organic carbon of lake sediment is a function of transport (for terrestrial organic matter), supply of inorganic material from the catchment, initial production of biomass, and the subsequent degree of degradation that the biomass is subject to. The interactions of these factors are often complex and can potentially obscure the interpretation of %OC data. Additionally, %OC can vary greatly between locations as a result of the interactions of these factors. In this study %OC is expressed as a weight/weight ratio and is therefore potentially subject to dilution by minerogenic contributions from the catchment. To fully interpret %OC data it is often useful to also examine the isotopic composition of the organic fraction of sediments as well as the ratio of carbon to nitrogen of paired samples. From the data presented below, it becomes clear that the organic matter preserved in Lower Sermilik is a combination of algal and C_3 plant contributions.

4.1.2 Sources of Organic Matter in Lower Sermilik

The organic carbon present in Lower Sermilik has been produced by a combination of vascular, C_3 land plants and lacustrine algae. This has been elucidated by analysis of the carbon to nitrogen ratio of discrete sediment samples and the carbon isotopic composition of the organic fraction of discrete sediment samples throughout the Lower Sermilik core. The values of the atomically corrected C/N ratio mostly occur between 12 and 18, which are too high for lacustrine algae and too low for the majority of C_3 plants (e.g. Meyers 1993, Meyers 1997, Meyers 2003).Similarly, the isotopic

composition of the organic carbon present in the Lower Sermilik core exhibits values common to both vascular plants and lacustrine algae. Thus, the bulk geochemical data indicate that both algae and C_3 plants are likely the largest contributors of organic carbon to Lower Sermilik, and that C_4 plants do not appear to play a notable role in contributing organics to Lower Sermilik at any point during the Holocene. These data also confirm that fluvial processes must be occurring throughout the Holocene in order to transport the remains of vascular land plant material from the catchment and into Lower Sermilik.

4.2 Biogenic Silica (BSi)

Biogenic silica, the siliceous material incorporated into the cell walls of diatoms may be used as a direct proxy for levels of paleo-productivity of diatoms (Conley 1988). Much like organic carbon expressed as a weight/weight percent, percent biogenic silica records are susceptible to dilution by intense sedimentation rates. Fortunately, Lower Sermilik is inferred to have been host to large populations of diatoms through the Holocene, and the overprinting of biogenic silica with clastic debris signals seems unlikely to have played a significant role. Even if overprinting of the biogenic silica record were a concern, the relative amount of biogenic silica in the Lower Sermilik sediments would still be useful due to the more or less stable accumulations rates. Additionally, warmer periods at Lower Sermilik are associated with lower surface runoff, and any alteration to the biogenic silica record would likely only exaggerate the signal of %BSi.

Previous studies of varved sediments have calibrated biogenic silica percentages to temperature (McKay et al. 2008), and a number of other studies have produced records of biogenic silica that closely track large scale temperature variations (e.g. Wagner et al.

2000). In this study %BSi is observed to be greatest during periods associated with stability and warmth (e.g. the Holocene Climatic Optimum).

4.3 X-ray fluorescence scanning

High resolution x-ray fluorescence scanning is a valuable tool for paleolimnologic reconstructions as it allows for interpretation of sediment sources, depositional rates, and modes of transport on very fine timescales. In this study the resolution of the XRF scans is many times greater than any other measurement and while fascinating proved to be unhelpful for interpretations beyond general trends without applying smoothing curves. The largest issue encountered while obtaining elemental profiles was machine drift. The core section LSRM-10G-B2 was scanned months after the rest of the Lower Sermilik core sections but under the same parameters, and while the general trends were preserved the values were nearly half of what they most likely should have been (this zone is outlined by a red rectangle in Figure 4**).** That being said, elemental ratios obtained by XRF scanning represent an extremely useful form of proxy for inferring a number of conditions. In addition to the analysis of several discrete elements this study makes use of two such elemental ratios: silica to potassium and manganese to iron.

4.3.1) Silica to Potassium

The ratio of silica to potassium is used in this catchment to infer periods of heightened bedrock weathering and erosion. Weathering of bedrock, including weathering of feldspar, produces clays minerals; hydrous aluminum phylosilicates containing variable amounts of cations including alkali metals and alkaline earth metals. The bedrock of Sermilik Valley is composed of basic charnockite and granite gneiss, both of which include alkaline earth metals (e.g. calcium, strontium) and alkali metals (e.g.

potassium, rubidium) as major constituents of their primary minerals. For example, phenocrysts of potassium feldspar were frequently noted while conducting field work in Sermilik Valley (Figure 15). Additionally, books of muscovite, of which potassium is a major constituent, were also discovered and collected in Sermilik Valley. Therefore, weathering of the charnockite and garnet gneiss complexes in Sermilik valley is speculated to generate potassium-rich clays, which are transported into Lower Sermilik via fluvial processes. Other processes, notably eolian, actively transporting minerogenic material with comparably high ratios of silica to potassium into Lower Sermilik during time of clay mineral production would be overwhelmed by the sheer availability of potassium-rich clays.

Figure 15. Phenocrysts of potassium-feldspar (orthoclase) found near Lower Sermilik. Such samples were highly abundant. Rock hammer for scale.

4.3.2) Manganese to Iron

The ratio of manganese to iron can be used to infer the relative oxygenation of bodies of water. Both iron and manganese share a negative relationship with dissolved oxygen, however under anoxic conditions manganese is rapidly reduced, resulting in a lower ratio of Mn to Fe (e.g. Davidson et al. 1982). Modern day oxygen levels in Lower Sermilik are high throughout the water column (Figure; however the Mn/Fe ratio of historic sediments from Lower Sermilik suggests sub-oxic conditions may have persisted for an extended period of time beginning around the onset of neoglaciation at 3450 cal yr BP.

4.4 Unit I (348-284 cm; ~7700-6900 cal yr BP): Deglaciation/Holocene Climatic Optimum transition

Following the emergence of Lower Sermilik from beneath the perennial ice of Sermilik Valley at approximately 7700 cal yr BP, the catchment of Lower Sermilik was a high-energy glaciofluvial environment characterized by the deposition of inorganic glacial detritus composed of coarse sand and cobbles. This phase of the Lower Sermilik catchment development is recorded in the sediment record from the base of the composite core at 348 centimeters to 284 cm (7700 cal yr BP until 6900 cal yr BP). Early on in this phase a strong proximal glacial influence dominates the sediment record. It was not until 7500 cal yr BP (325cm) that pelagic sedimentation began, and the influence of ice persisting in Sermilik Valley lessened. This most likely occurred after the ice persisting in the valley retreated into the elevated cirque to the North of Lower Sermilik and beyond the bedrock ridge dividing Upper Sermilik from Lower Sermilik.

4.4.1) Geochemical Evidence

The glaciofluvial conditions in Sermilik Valley were likely unsupportive of biological activity. Percent organic carbon of sediments deposited during this phase is very low (<0.05%), with paired C/N values reflecting an entirely algal source for the small amount of organic material present (Figure 14). It is possible that because these samples were not acidified to remove inorganic carbon prior to analysis that this small percentage of carbon is actually reflecting a background signal of inorganic carbon present in the catchment, however a small population of diatoms inferred from biogenic silica values are also associated with this phase, which suggests that these carbon values are indeed indicative of a small algal presence. $\delta^{13}C$ values for this phase exhibit high variability in comparison to much of the Lower Sermilik record and range from -26‰ to -30‰ . Though these shifts may reflect changes in organic matter sources or ecosystem shifts, this range of values is indicative of both C_3 plant organic matter and algal organic matter. $\delta^{15}N$ does not reflect values typical of algal production. The high flushing rate of Lower Sermilik, the low mean %OC, and lack of evidence for aquatic plant populations all suggest that nitrogen available in the form of nitrate had neither the time nor means to be enriched significantly by recycling before being diluted and replaced by fresh atmospheric nitrogen. This hypothesis is supported by the overall lack of variation seen the $\delta^{15}N$ values of the Lower Sermilik sediment record.

4.4.2) X-ray fluorescence scanning evidence

As may be expected, the coarse and highly minerogenic basal debris of the Lower Sermilik core is characterized by elevated counts per second measured in most major elements (Figure 11). The inferred abundancies of these elements may be explained by

the large amount of mineral-rich debris made available by mechanical weathering of the basic charnockite and garnet gneiss geologic units in and around the Lower Sermilik catchment. During this period the influx of these glacial sediments by fluvial processes and meltwater runoff (e.g. physical transport of sediment, chemical leaching of tills) dominated the depositional processes. Other modes of transport, such as eolian processes, acting on the catchment likely carried debris with proportionally different suites of elements. Unfortunately, evidence of these processes is not available during this phase of the Lower Sermilik catchment development, most likely due to overprinting by the extremely proximal and robust glaciofluvial sediment supply.

The ratio of silica to potassium in Unit I is may indicate the extent of erosional processes acting on the catchment. Initially low, Si/K values outside of the basal debris rose steadily until the boundary of Unit I and Unit II. This signal is interpreted to indicate a gradual decrease in the availability of potassium feldspar-rich sediments (e.g. glacial clays) made available by the mechanical weathering of charnockite and granite gneiss, and the slow transition to a system less-dominated by glacial detritus. This is supported by decreases observed in the counts of other elements strongly associated with charnockite and granite gneiss, such as manganese, calcium, and titanium. As an aside, it is important to note that while these elements are sometimes associated with mafic rocks, the abundances of these elements can perhaps be tied to the orthopyroxines of the basic charnockite underlying the majority of Sermilik Valley. Orthopyroxines have the general formula $XY(Si,Al)_2O_6$, where X may represent elements such as calcium, sodium, and magnesium, and Y may represent calcium, manganese, and titanium. Calcium may also owe some abundance to the presence of plagioclase in the catchment.

The high ratio of manganese to iron, which has been widely used as a proxy for oxic/anoxic conditions at the sediment-water interface (e.g. Spofforth et al. 2008) in this unit may be suggesting fully oxygenated bottom waters due to a general lack of biological activity in the lake. Although this is a convenient explanation, it is equally if not more likely that the high ratio of manganese to iron is due to the high abundance of manganese found in the glacial debris at the bottom of Unit I relative to iron. Thus the Mn/Fe ratios of Unit I probably do not reflect oxygenation of Lower Sermilik very well due to manganese-rich clasts.

4.5) Unit II (284-139 cm; ~6900-3450 cal yr BP): Holocene Climatic Optimum

The transition from the glaciofluvial environment of Unit I to Unit II is rapid and clearly expressed by bulk geochemistry of sediments, elemental profiles acquired by XRF scanning, and in a visible lithologic shift to fine, organic-rich laminations. Unit II extends from 284 through 139 cm (~6900 to 3450 cal yr BP) and is interpreted to represent the Holocene Climatic Optimum as expressed in Sermilik Valley based on the abundance of paleo-diatom populations and organic carbon content preserved in the sediments of this unit.

Previous work (e.g. Wagner et al. 2000) on the Holocene climate history of East Greenland suggests that during the period of time expressed in Unit II East Greenland experienced an extended period of stable warmth, though beginning around 4500 years BP temperatures begin to steadily decline until neoglacial conditions were achieved. Additionally, previous reconstructions of humidity in East Greenland indicate a transition

from arid conditions to greater amounts of precipitation beginning around 7000 cal yr BP, reaching maxima around 3500 cal yr BP (Wager et al. 2000).

4.5.1) Geochemical Evidence

Environmental conditions in Sermilik Valley at the beginning of Unit II are interpreted to have been warm with a possible trend towards increasing precipitation. It is quite possible that atmospheric temperatures were already at Holocene Climatic Optimum (HCO) levels during the deposition of much of Unit I, however conditions for supporting and/or preserving biological signals were clearly not at an optimum in Lower Sermilik due to the proximal influence of large quantities of glacial ice. Nonetheless, evidence for increased warmth is seen in the biogenic silica record of Lower Sermilik starting after 6900 cal yr BP. Biogenic silica percentages are interpreted to reflect directly the paleo-diatom populations, which in turn are interpreted to strongly reflect temperature conditions. At the onset of Unit II the population of diatoms in Lower Sermilik is observed to increase rapidly to high and consistent values. Diatom populations appear to have thrived in abundance throughout the Holocene Climatic Optimum, though beginning around 4000 cal yr BP populations began to decrease in a stepwise fashion. This population decline may be in response to decreasing temperatures, although it is also possible that increases in precipitation at this time resulted in the overprinting of biogenic silica values due to the increased deposition of minerogenic materials from the catchment.

Percent organic carbon experienced an unprecedented peak, rising from <0.5% to >2.5% at the transition between Unit I and Unit II. Atomically corrected C/N ratios

indicate the source of this organic matter is a mix of algal and terrestrial C3 plant material with a tendency towards a slightly more dominant algal source. The abrupt peak of organic carbon at the base of Unit II quickly returned to a mean baseline of ~2% OC over several centimeters. An explanation for this abrupt rise and fall may be catchment instability. The lack of stable topsoil and mattes of vegetation would have made transport of organic matter from the catchment into Lower Sermilik much easier. If increased transport of material into Lower Sermilik due to an unstable catchment were the case then the spike in organic carbon may have been compounded by increased export of phosphorus, from the unstable catchment (a common limiting factor of autochthonous production) resulting in algal blooms.

4.5.2) XRF Scanning Evidence

Elemental profiles generated for Unit II are distinct from those of Unit I. Elements associated with clay minerals such as titanium, calcium, and potassium underwent a marked decrease in counts throughout the majority of the HCO. This is thought to be due to a lower abundance of glacially-eroded material, and also in part to the higher abundance of organic material in the sediments. This is further supported by the ratio of silica to potassium, which when high is interpreted to reflect periods of little-to-no glacial influence on the Lower Sermilik catchment. Similarly, low values for the ratio of manganese to iron indicate that Lower Sermilik was less oxygenated during this period of the Holocene. This is concordant with increased populations of living organisms that consume oxygen, and the consumption of oxygen during the oxidation of decaying matter.

4.6) Unit III (139-0 centimeters, or 3450 to -60 cal yr BP): Neoglaciation through Modern

Unit III extends from 139 cm (3450 cal yr BP) to 0 cm (interpolated -60 cal yr BP). The transition from the Holocene Climatic Optimum into neoglaciation at the boundaries of Unit II and Unit II is expressed clearly in the bulk geochemical data, and in the Si/K ratio. The transition is apparent but not as a clear-cut in visible lithology, individual elemental profiles, and in the Mn/Fe ratio. The onset of neoglaciation is inferred to be a period of cool temperatures and high precipitation, with possible climate anomalies occurring approximately from 1300 cal yr BP to 410 cal yr BP and from 370 to 227 cal yr BP --the former, possibly an anomalous warming trend, and the latter possibly an anomalous cooling trend.

4.6.1) XRF scanning evidence

Environmental conditions in Sermilik Valley at the beginning of Unit III are interpreted as having been cool and wet. Coincident with the timing of neoglaciation suggested by this study is the appearance of the Mittivakkat Glacier (Humlum et al. 2008). This date assigned by Humlum et al. 2008 supported by the XRF scanning data presented in this thesis, which suggests significant amounts of rock flour began entering Upper Sermilik and Lower Sermilik around this time. Mittivakkat today is the largest contiguous ice field on Ammassalik Island, discharging melt water and debris into Sermilik Fjord to the west, and into Upper Sermilik Lake to the Southeast. As the result, modern-day Upper Sermilik is a vivid turquoise color and displays an enormous plume of suspended sediment. This sediment plume has been captured numerous times in historical

satellite imagery, and was observed by the author in July of 2012. Large quantities of the perpetually suspended glacially-derived sediment observed in Upper Sermilik are thought to be carried into Lower Sermilik by a narrow, rapidly flowing channel. This is supported by the general rise in elements associated with glacial clays seen in the Lower Sermilik sediment record at this time. Further evidence is supplied by the Si/K ratio, which shows a sharp decline at this time, indicating a transition back into sediments containing larger quantities of potassium-rich clays.

The ratio of manganese to iron experiences a negative excursion at the onset of neoglaciation, which coincides with abrupt increases in the amount of organic carbon preserved in the sediment record. This excursion is interpreted as a period of sub-oxic conditions in Lower Sermilik brought on by periods of extended seasonal ice cover limiting wind-mixing of the surface layer, and by of the oxidation of the large influxes of organic matter.

4.6.2) Geochemical Evidence

At the onset of neoglaciation the %OC preserved in the Lower Sermilik sediment record abruptly increases to over 3%. This first peak coincides with a slight increase in the C/N ratio, indicating a slightly higher proportion of C_3 plants contributing organic matter to Lower Sermilik record. This is interpreted to represent the gradual destabilization of the Lower Sermilik catchment via cold temperatures and increased precipitation. This may have also resulted in the delivery of increased nutrients to Lower Sermilik resulting in increased algal productivity. After the initial peak in organic carbon, a brief period of extremely low %OC persisted before again rising to three distinct and

short-lived peaks. These peaks are associated with C/N excursions towards higher values indicating more terrestrial input into Lower Sermilik. These periods are interpreted to represent the influx of terrestrial organic matter in streams to Lower Sermilik.

After ~1500 cal yr BP %OC experienced extremely stable conditions for duration of the sediment core. This period is marked by a steady rise in mean C/N values until the final 20 cm of the core when values drop to roughly 10. These geochemical data are interpreted to indicate a shift from a dominantly algal source of organic matter to a much more mixed signal, possibly as the result of new, dominant post-glacial plant species.

The population of diatoms in Unit III experienced saw tooth-like variability with consistently low mean values until 1300 cal yr BP when values begin to increase until ~410 cal yr BP. In a general sense the timing of this positive trend coincides with the expected timing of the Medieval Climate Anomaly, however the signal is not exceptionally strong in this record and to identify this as a specific event may be overzealous. From 370 until 227 cal yr BP the population of diatoms in Lower Sermilik experienced an abrupt and extreme decline. This drop may be attributable to the Little Ice Age. Unfortunately there is no data other than the record of biogenic silica to support this.

CHAPTER 5

CONCLUSION

Based upon the evaluation of the Lower Sermilik sediment record by analyses of bulk geochemistry and high-resolution scans it can be concluded from this study that climate variability is captured in the sediment record of Lower Sermilik. Though clear large-scale climate signals can be identified in this record, there remains a great deal of obfuscation of details by background noise created by high inputs of minerogenic materials. In addition to this background noise, mass wasting deposits were found throughout the core, making continuous assessment of unfragmented core sections impossible. However all things considered, the Lower Sermilik record contributes to the greater understanding of Holocene climate variability in Eastern Greenland and will undoubtedly contribute to the interpretations of other lake-based climate reconstructions presently taking place in Eastern Greenland.

Future work will include the re-scanning of the sediment core sections lacking data using the Itrax XRF core scanner. Additional evaluation of the silica to potassium ratio is also necessary in order to determine the influence of biogenic silica on this dataset. Finally, a major boon to this study will be the acquisition of grain-size data. Grain size will be extremely helpful in identifying turbidites in a quantifiable manor, as well as for determining the abundance of clays throughout the composite core.

BIBLIOGRAPHY

Alley, R., Mayewski, P., Sowers, T., Stuiver, M., Taylor, K., Clark, P., 1997. Holocene climatic instability: A prominent, widespread event 8200 yr ago. Geology 25, 483-486.

Anderson, N., Liverside, A., McGowan, S., Jones, M., 2012. Lake and catchment response to Holocene environmental change: spatial variability along a climate gradient in southwest Greenland. J Paleolimnology 48, 209-222.

Andresen, C., Bjorck, S., Bennike, O., Bond, G., 2004. Holocene climate changes in Southern Greenland: evidence from lake sediments. Journal of Quaternary Science 19, 783-795.

Axford, Y., Losee, S., Briner, J., Francis, D., Langdon, P., Walker, I., 2013. Holocene temperature history at the western Greenland Ice Sheet margin reconstructed from lake sediments. Quaternary Science Reviews 59, 87-100.

Bitz, C., Ridley, J., Holland, M., Cattle, H., 2010. Global climate models and 20th and 21st century Arctic climate change. Arctic Climate Change –the ACSYS Decade and Beyond (Ed. P. Lemke).

Blaauw, M., 2010. Methods and code for 'classical' age-modeling of radiocarbon sequences. Quaternary Geochronology xxx (online), 1-7.

Blass, A., Bigler, C., Grosjean, M., Sturm, M., 2007. Decadal-scale autumn temperature reconstruction back to AD 1580 inferred from the varved sediments of Lake Silvaplana (southeastern Swiss Alps). Quaternary Research 68, 184-195.

Bridgwater, D., 1976. Nagssustoqidian mobile belt in East Greenland. Geology of Greenland 7, 97-103.

Briner, J., Stewart, H.A.M., Young, N.E., Phillips, W., Losee, S., 2010. Using proglacial-threshold lakes to constrain fluctuations of the Jakobshavn Isbrae ice margin, western Greenland, during the Holocene. Quaternary Science Reviews 29, 3861-3874.

Broeker, W., Denton, G., 1989. The role of ocean-atmosphere reorganizations in glacial cycles. Geochimica et Cosmochimica Acta 53, 2465-2501.

Callaghan, T., Bergholm, F., Christensen, T., Jonasson, C., Kokfelt., U., Johansson, M., 2010. A new climate era in the sub-Arctic: Accelerating climate changes and multiple impacts. Geophysical Research Letters 37, L14705.

Cappelen J, Laursen EV, Jörgensen, PV, Kern-Hansen C, 2011. DMI monthly climate data collection 1768–2010, Denmark, The Faroe Islands and Greenland. *DMI Technical Report 11-05*. Copenhagen, Ministry of Climate and Energy, p. 54.

Castañeda, I., Schouten, S., 2011. A review of molecular organic proxies for examining modern and ancient lacustrine environments. Quaternary Science Reviews 30, 2851-2891.

Christiansen, H., Murray, A., Mejdahl, V., Humlum, O., 1999. Luminescence dating of Holocene geomorphic activity on Ammassalik Island, SE Greenland. Quaternary Geochronology 18, 191-205.

Clark, P., Pisias, N., Stocker, T., Weaver, A., 2002. The role of thermohaline circulation in abrupt climate change. Nature 415, 863-869.

Colman, S., Peck, J., Hatton, J., Karabanov, E., King, J., 1999. Biogenic silica records from the BDP93 drill site and adjacent areas of the Selenga Delta, Lake Baikal, Siberia. J Paleolimnol 21, 9-17.

Conley, D., 1988. Biogenic Silica as an Estimate of Siliceous Microfossil Abundance in Great Lakes Sediments. Biogeochemistry 6, 161-179.

Cremer, H., Melles, M., Wagner, B., 2001. Holocene climate changes reflected in a diatom succession from Basaltø, East Greenland. Can. J. Bot. 79, 649-656.

D'Andrea, W., Huang, Y., Fritz, S., Anderson, N.J., 2011. Abrupt Holocene climate change as an important factor for human migration in West Greenland. PNAS 108, 9765-9769.

De Jong, S., 1993. SIMPLS: an alternative approach to partial least squares regression. Chemometrics and Intelligent Laboratory Systems 18, 251–263.

Dowdeswell, J., Uenzelmann-Neben, G., Whittington, R., Marienfeld, P., 1994. The Late Quaternary sediment record in Scoresby Sund, East Greenland. Boreas 23, 294-310.

Fogel, M. L., & Cifuentes, L. A. (1993). Isotope fractionation during primary production. Organic geochemistry, 73-98.

Funder, S., Hansen, L., 1996. The Greenland ice sheet – a model for its culmination and decay during and after the last glacial maximum. Bulletin of the Geological Society of Denmark 42, 137-152.

Funder, S., Hjort, C., Landvik, J., Man, S., Ree, N., Stein, R., 1998. History of a stable ice margin- East Greenland during the Middle and Upper Pleistocene. Quaternary Science Reviews 17, 77-125.

Geirsdottir, A., Hardardottir, J., Andrews, J., 2000. Late-Holocene terrestrial glacial history of Miki and I.C. Jacobsen Fjords, East Greenland. The Holocene 10, 123-134.

Gendron-Badou, A., Coradin, T., Maquet, J., Frohlich, F., Livage, J., 2003. Spectroscopic characterization of biogenic silica. Journal of Non-Crystalline Solids 316, 331-337.

Gregory, J., Huybrechts, P., Raper, S., 2004. Threatened loss of the Greenland ice-sheet. Nature 428, 616.

Griffiths, P. R., & de Haseth, J. A. (1986). Fourier Transform Infrared Spectrometry John Wiley & Sons. New York, 340.

Hakansoon, L., Briner, J., Alexandersson, H., Aldahand, A., Possnerte, G., 2007. 10Be ages from central east Greenland constrain the extent of the Greenland ice sheet during the Last Glacial Maximum. Quaternary Science Reviews 26, 2316-2321.

Hanna, E., Cappelen, J., Fettweis, X., Huybrechts, P., Luckman, A., Ribergaard, M., 2009. Hydrologic response of the Greenland ice sheet: the role of oceanographic warming. Hyrol. Process 23, 7-30.

Hasholt, B., Mernild, S., 2008. Hydrology, sediment transport and water resources of Ammassalik Island, SE Greenland. Danish Journal of Geography 108, 73-95.

Hodell, D. A., & Schelske, C. L. (1998). Production, sedimentation, and isotopic composition of organic matter in Lake Ontario. Limnology and Oceanography, *43*(2), 200-214.

Humlum, O., Christiansen, H., 2008. Geomorphology of the Ammassalik Island, SE Greenland. Danish Journal of Geography 108, 5-20.

Hurrell, J. W., Kushnir, Y., Ottersen, G., & Visbeck, M. (2003). The North Atlantic Oscillation: climatic significance and environmental impact (Vol. 134, pp. 1-279). American Geophysical Union.

Hurrell, J., Deser, C., 2009. North Atlantic climate variabililty: the role of the North Atlantic Oscillation. Journal of Marine Systems 78, 28-41.

Jakobsen, B., Fredskild, B., Pedersen, J., 2008.Holocene changes in climate and vegetation in the Ammassalik area, East Greenland, recorded in lake sediments and soil profiles. Danish Journal of Geography 108, 21-50.

Johnsen, S., Dahl-Jensen, D., Gundestrup, N., Steffensen, J., Clausen, H., Miller, H., Masson-Delmotte, V., Sveinbjörnsdottir, A., White, J., 2001. Oxygen isotope and paleotemperature records from six Greenland ice-core stations: Camp Century, Dye-3, GRIP, GISP2, Renland, and NorthGRIP. Journal of Quaternary Science 16, 299-307.

Jennings, A., Andrews, J., Wilson, L., 2011. Holocene environmental evolution of the Se Greenland Shelf North and South of the Denmark Strait: Irminger and East Greenland current interactions. Quaternary Science Reviews 30, 980-998.

Justwan., A., Koc, N., Jennings, A., 2008. Evolution of the Irminger and East Icelandic Current systems through the Holocene, revealed by diatom-based sea surface temperature reconstructions. Quaternary Science Reviews 27, 1571-1582.

Kaplan, M., Wolfe, A., Miller, G., 2002. Holocene Environmental Variability in Southern Greenland Inferred from Lake Sediments. Quaternary Research 58, 149-159.

Kaplan, M., Wolfe, A., 2006. Spatial and temporal variability of Holocene temperature in the North Atlantic Region. Quaternary Research 65, 223-231.

Kattsov, V., Kallen, E., Cattle, H., Christensen, J., Drange, H., Hanseen-Baurer, I., Johannesen, T., Karol, I., Raisanen, J., Svensson, G., Vavulin, S., 2007. Future Climate Change: Modeling and Scenarios for the Arctic. Arctic Climate Impacts Assesment (ACIA).

Kaufman, D., Schneider, D., McKay, N., Ammann, C., Bradley, R., Briffa, K., Miller, G., Otto-Bliesner, B., Overpeck, J., Vinther, B., Arctic Lakes 2k Project Members, 2009. Recent Warming Reverses Long-Term Arctic Cooling. Science 325, 1236-1239.

Kaufman, D., Ager, T., Anderson, N., Anderson, P., Andrews, J., Bartlein, P., Brubaker, L., Coats, L., Cwynar, L., Duvall, M., Dyke, A., Edwards, M., Eisner, W., Gajewski, K., Geirsdottir, A., Hu, F., Jennings, A., Kaplan, M., Kerwin, M., Loshkin, A., MacDonald, G., Miller, G., Mock, C., Oswald, W., Otto-Bliesner, B., Porinchu, D., Ruhland, K., Smol, J., Steig, E., Wolfe, B., 2004. Holocene Thermal Maximum in the western Arctic (0-180°W). Quaternary Science Reviews 23, 529-560.

Kaushal, S., & Binford, M. W. (1999). Relationship between C: N ratios of lake sediments, organic matter sources, and historical deforestation in Lake Pleasant, Massachusetts, USA. Journal of Paleolimnology, *22*(4), 439-442.

Kelly, M., Lowell, T., Hall, B., Schaefer, J., Finkel, R., Goehring, B., Alley, R., Denton, G., 2008. A 10Be chronology of lateglacial and Holocene mountain glaciation in the Scoresby Sund region, east Greenland: implications for seasonality during late glacial time. Quaternary Science Reviews 1-10.

Klug, M., Schmidt, S., Bennike, O., Heiri, O. Melles, M., Wagner, B., 2008. Lake sediments from Store Koldewey, Northeast Greenland, as archive of Lake Pleistocene and Holocene climatic and environmental changes. Boreas, 59-71.

Klug, M., Bennike, O., Wagner, B., 2009. Repeated short-term bioproductivity changes in a coastal lake on Store Koldewey, northeast Greenland: an indicator of varying sea ice coverage? The Holocene, 19, 653-663.

Kobashi, T., Kawamura, K., Severinghaus, J., Barnola, J., Nakaegawa, T., Vinther, B., Johnsen, S., Box, J., 2011. High variability of Greenland surface temperature over the past 4000 years estimated from trapped air in an ice core. Geophysical Research Letters 38, L21301.

Kuijpers, A., Troelstra, S., Prins, A., Linthout, K., Akhmetzhaov, A., Bouryak, S., Bachmann, M., Lassen, S., Rassmussen, S., Jensen, J., 2003. Late Quaternary sedimentary processes and ocean circulation changes at the Southeast Greenland margin. Marine Geology 195, 109-129.

Kutzbach, J., Guetter, P., 1986. The influence of changing orbital parameters and surface boundary conditions on climate simulations for the past 18,000 years. Journal of the Atmospheric Sciences 43, 1726-1759.

Landvik, J., 1994. The last glaciation of Germania Land and adjacent areas, northeast Greenland. Journal of Quaternary Science 9, 81-92.

Last, W., Smol, J., 2001. Tracking Environmental Change Using Lake Sediments, Volume 2: Physical and Geochemical Methods. Kluwer Academic Publishers, Dordrecht, The Netherlands.

Lopez, P. Navarro, E., Ordonez, J., Caputo, L., Armengol, J., 2006. Elemental ratios in sediments as indicators of ecological processes in Spanish reservoirs. Limnetica 25, 499-512.

Marcott, S., Shakun, J., Clark, P., Mix, A., 2013. A reconstruction of Regional and Global Temperature for the past 11,300 years. Science 339, 1198-1201.

Massa, C., Perren, B., Gauthier, E., Bichet, V., Petit, C., Richard, H., 2012. A multiproxy evaluation of Holocene environmental change from Lake Igaliku, South Greenland. J Paleolimnology 48, 241-258.

Masson-Delmotte, V., Swingedouw, D., Landais, A., Seidenkrantz, M., Gauthier, E., Bichet, V., Massa, C., Perren, B., Jomelli, V., Adalgeirsdottir, G., Christensen, J., Arneborg, J., Bhatt, U., Walker, D., Elbering, B., Gillet-Chaulet, F., Ritz, C., Gallee, H., van den Broeke, M., Fettweis, X., de Vernal, A., Vinther, B., 2012. Greenland climate change: from the past to the future. WIREs Clim Change 10.1002/wcc.186.

Mayeweski, P., Rohling, E., Stager, C., Karlen, W., Massch, K., Meeker, D., Meyerson, E., Gasse, F., van Kreveld, S., Holmgren, K., Lee-Thorp, J., Rosqvist, G., Rack, F., Staubwasser, M., Schneider, R., Steig, E., 2004. Holocene Climate Variability. Quaternary Research 62, 243-255.

McGowan, S., Ryves, D., Anderson, N.J., 2003. Holocene records of effective precipitation in West Greenland. The Holocene 13, 239-249.

McKay, N., Kaufman, D., Michelutti, N., 2008. Biogenic silica concentration as a high-resolution, quantitative temperature proxy at Hallet Lake, south-central Alaska. Geophysical Research Letters 35.

Mernild, S., Seidenkrantz, P, Liston, G, Hasholt, B., 2011. Climate-driven fluctuations in freshwater flux to Sermilik Fjord East Greenland, during the last 4000 years. The Holocene 22, 155-164.

Meyers, P. 2003. Applications of organic geochemistry to paleolimnological reconstructions: a summary of examples from the Laurentian Great Lakes. Organic Geochemistry 34, 261-289.

Meyers, P. 1997. Organic geochemical proxies for paleoceanographic, paleolimnologic, and paleoclimatic processes. Organic Geochemistry 27, 213-250.

Meyers, P., Ishiwatari, R., 1993. Lacustrine organic geochemistry – an overview of indicators of organic matter sources and diagenesis in lake sediments. Org. Geochemistry 20, 867-900.

Moenke H., 1974. Silica,the three-dimensional silicates, borosilicates and beryllium silicates. Mineralogical Society Monograph 4, 365-379.

Moritz, R. E., Bitz, C. M., & Steig, E. J. (2002). Dynamics of recent climate change in the Arctic. Science, 297(5586), 1497-1502.

Mortlock, R., Froelich, P., 1989. A simple method for the rapid-determination of biogenic opal in pelagic marine-sediments. Oceanographic research papers 36, 1415-1426.

Olsen, J., Anderson, N.J., Knudsen, M., 2012. Variability of the North Atlantic Oscillation over the past 5,200 years. Nature Geoscience 5, 808-812.

Overland, J., Wang, M., Salo, S., 2008. The recent Arctic warm period. Tellus 60A, 589-597.

Perren, B., Anderson, J., Douglas, M., Fritz, S., 2012. The influence of temperature, moisture, and eolian activity on Holocene lake development in West Greenland. J Paleolimnology 48, 223-239.

Peterson, B., Howarth, R., 1987. Sulfur, carbon, and nitrogen isotopes used to trace organic matter flow in the salt-marsh estuaries. Limnology and Oceanography 32, 1195-1213.

Reimer, P. J., Baillie, M. G., Bard, E., Bayliss, A., Beck, J. W., Blackwell, P. G., ... & Weyhenmeyer, C. E. (2009). IntCal09 and Marine09 radiocarbon age calibration curves, 0-50,000 yeats cal BP.

Roberts, D., Long, A., Schnabel, C., Freeman, S., Simpson, M., 2008. The deglacial history of southeast sector of the Greenland Ice Sheet during the Last Glacial Maximum. Journ. Quart. Sci. Rew.

Rosén, P., Vogel, H., Cunningham, L., Reuss, N., Conley, D., Persson, P., 2010. Fourier transform infrared spectroscopy, a new method for rapid determination of total organic and inorganic carbon and biogenic silica concentration in lake sediments. J Paleolimnol 43, 247-259.

Serreze, M., Barrett, A., Stroeve, J., Kindig, D., Holland, M., 2009. The emergence of surface-based Arctic amplification. The Cryosphere 3, 11-19.

Smol, J., Cumming, B., 2000, Tracking Long-Term Changes in Climate using Algal Indicators in Lake Sediments. J. Phycol 36, 986-1011.

Steffen, K., Box, J., 2001. Surface climatology of the Greenland ice sheet: Greenland Climate Network 1995-1999. Journal of Geophysical Research 100.

Stein, R., Nam, S., Grobe, H., Hubberten, H., 1996. Late Quaternary glacial history aand short-term ice-rafted debris fluctuations along the East Greenland continental margin. In: Andrews, J., Austin, W., Bergsten, H., Jennings, A., (eds.), Late Quaternary Paleoceanography off the North Atlantic Margins. Geological Society, London, Special Publication 111: 135-151.

Stuiver, M., & Reimer, P. J. (1993). Radiocarbon Calibration Program, Revised 3.0. 3. Seattle: University of Washington Quaternary Isotope Laboratory.

Sutherland, D., Pickart, R., 2008. The East Greenland Current: Structure, variability, and forcing. Progress in Oceanography 78, 58-77.

Swann, G., Mackay, A., 2006. Potential limitations of biogenic silica as an indicator of abrupt climate change in Lake Baikal, Russia. J Paleolimnol 36, 81-89.

Talbot, M. R., & Johannessen, T. (1992). A high resolution palaeoclimatic record for the last 27,500 years in tropical West Africa from the carbon and nitrogen isotopic composition of lacustrine organic matter. Earth and Planetary Science Letters, 110(1), 23-37.

Talbot, M. R. (2002). Nitrogen isotopes in palaeolimnology. In Tracking environmental change using lake sediments (pp. 401-439). Springer Netherlands.

Thomas, E., Wolff, E., Mulvaney, R., Steffensen, J., Johnsen, J., Arrowsmith, C., White, J., Vaughn, B., Popp, T., 2007. The 8.2 ka event from Greenland ice cores. Quaternary Science Reviews 26, 70-81.

Trouet, V., Esper, J., Graham, N., Baker, A., Scourse, J., Frank, D., 2009. Persistent Positive North Atlantic Oscillation Mode Dominated the Medieval Climate Anomaly. Science 324, 78-80.

Vinther, B., Buchardt, S., Clausen, H., Dahl-Jensen, D., Johnsen, S., Fisher, D., Koerner, R., Raynaud, D., Lipenkov, V., Andersen, K., Blunier, T., Rasmussen, O., Steffensen, J., Svensson, A., 2009. Holocene thinning of the Greenland ice sheet. Nature 461, 385-388.

Vinther, B., Clausen, H., Fisher, D., Koerner, R., Johnsen, S., Andersen, K., Dahl-Jensen, D., Rasmussen, S., Steffensen, J., Svensson, A., 2008, Synchronizing ice cores from the Renland and Agassiz ice caps to the Greenland Ice Core Chronology. Journal of Geophysical Research, 113, D08115.

Vogel, H., Rosen, P., Wagner, B., Melles, M., Persson, P., 2008. Fourier transform infrared spectroscopy, a new cost-effective tool for quantitative analysis of biogeochemical properties in long sediment records. Journal of Paleolimnology 40, 689-702.

von Gunten, L., D'Andrea, W., Bradley, R., Huang, Y., 2012. Proxy-to-proxy calibration: Increasing temporal resolution of quantitative climate reconstructions. Scientific Reports 2, 10.1038/srep00609.

Wager, L., 1934. Geological investigations in East Greenland. I. General geology from Angmagsalik to Kap Dalton. Meddr Grøenland 105, 2-46.

Wagner, B., Melles, M., Hahne, J., Niessen, F., Hubberten, H., 2000. Holocene climate history of Geographical Society Ø, East Greenland- evidence from lake sediments. Paleoceanography, Paleoclimatology, Paleoecology 160, 45-68.

Wagner, B., Melles, M., 2002. Holocene environmental history of western Ymer Ø, East Greenland, inferred from lake sediments. Quaternary International 89, 156-176.

Wanner, H., Beer, J., Butikofer, J., Crowley, T., Cusbach, U., Fluckiger, J., Goosse, H., Grosjean, M., Joos, F., Kaplan, J., Kuttel, M., Muller, S., Prentice, C., Solomina, O., Stocker, T., Tarasov, P., Wagner, M., Widmann, M., 2008. Mid-to Late Holocene climate change: an overview. Quaternary Science Reviews, 1-38.

Willemse, N., Tornqvist, T., 1999. Holocene century-scale temperature variability from West Greenland lake records. Geology, 27. 580-584.

Williams, D., Peck, J., Karabanov, E., Prokopenko, A., Kravchinsky, V., King, J., Kuzmin, M., 1997. Lake Baikal Record of Continental Climate Response to Orbital Insolation During the Past 5 Million Years. Science 278, 1114-1117.

Zwang, M., Munchow, A., 2006. Warming and freshening of Baffin Bay. J. Geophys Res Oceans 111:C7.